A SPECTRAL APPROACH FOR SOLVING TWO-FLUID FLOW STABILITY PROBLEM

A THESIS SUBMITTED TO
THE GRADUATE SCHOOL OF NATURAL AND APPLIED SCIENCES
OF
MIDDLE EAST TECHNICAL UNIVERSITY

BY

MEHMET EMIN ÇELIKKIRAN

IN PARTIAL FULFILLMENT OF THE REQUIREMENTS
FOR
THE DEGREE OF MASTER OF SCIENCE
IN
MECHANICAL ENGINEERING

FEBRUARY 2022

Approval of the thesis:

A SPECTRAL APPROACH FOR SOLVING TWO-FLUID FLOW STABILITY PROBLEM

submitted by **MEHMET EMIN ÇELIKKIRAN** in partial fulfillment of the requirements for the degree of **Master of Science in Mechanical Engineering Department, Middle East Technical University** by,

Prof. Dr. Halil Kalıpçılar
Dean, Graduate School of **Natural and Applied Sciences** _____

Prof. Dr. M.A. Sahir Arıkan
Head of Department, **Mechanical Engineering** _____

Prof. Dr. Hakan I. Tarman
Supervisor, **Mechanical Engineering, METU** _____

Examining Committee Members:

Assoc. Prof. Dr. Cüneyt SERT
Mechanical Engineering, METU _____

Prof. Dr. Hakan I. TARMAN
Mechanical Engineering, METU _____

Prof. Dr. M. Metin YAVUZ
Mechanical Engineering, METU _____

Assoc. Prof. Dr. Utku KANOĞLU
Engineering Sciences, METU _____

Assist. Prof. Dr. Sıtkı USLU
Mechanical Engineering, TOBB ETU _____

Date: 11.02.2022

I hereby declare that all information in this document has been obtained and presented in accordance with academic rules and ethical conduct. I also declare that, as required by these rules and conduct, I have fully cited and referenced all material and results that are not original to this work.

Name, Surname: Mehmet Emin Çelikkıran

Signature :

ABSTRACT

A SPECTRAL APPROACH FOR SOLVING TWO-FLUID FLOW STABILITY PROBLEM

Çelikkıran, Mehmet Emin
M.S., Department of Mechanical Engineering
Supervisor: Prof. Dr. Hakan I. Tarman

February 2022, 84 pages

Turbulence and transition to turbulence are still one of the unresolved topics in physics. Multiphase applications of the transitional flows are more complex than their single-phase counterparts due to having many options for the source of instability. From oceanography to rocket engines, from oil industry to astrophysical phenomena, multiphase instabilities have many examples in both nature and industry. Acquiring the knowledge of the starting point of transition is crucial in all these applications. In this study focus is the instability of multiphase flows, especially the instabilities at interfaces. Linear hydrodynamic stability approach is used, and the Orr-Sommerfeld equation is solved in order to capture the behavior of perturbations. For multiphase flow, Orr-Sommerfeld equations for each phase are built, and interface conditions are applied to connect individual phases. The Reynolds number is not the only dimensionless parameter for multiphase flows to affect the perturbations and instability. Stratifications of density and viscosity, the effect of surface tension, gravity, and derivatives of mean velocity profiles will all have characteristic effects on the instabilities at the interface. A spectral method, Chebyshev Collocation method, is used for discretization. Matlab, Octave, and C++ programming languages are used for valida-

tion cases. Validation of codes for both single-phase and multiphase flow is acquired by the comparison of numerical results and results from the literature.

Keywords: hydrodynamic instability, multifluid flow, spectral methods, eigenvalue problem

ÖZ

ÇİFT-AKIŞKANLI AKIŞ KARARLILIK PROBLEMİ ÇÖZÜMÜ İÇİN SPECTRAL METOT YAKLAŞIMI

Çelikkıran, Mehmet Emin
Yüksek Lisans, Makina Mühendisliği Bölümü
Tez Yöneticisi: Prof. Dr. Hakan I. Tarman

Şubat 2022 , 84 sayfa

Türbülans ve türbülansa geçiş, fizikte hala çözülmemiş konulardan biridir. Geçiş akışlarının çok fazlı uygulamaları, kararsızlık kaynağı için birçok seçeneğe sahip olduğundan, tek fazlı muadillerine göre daha karmaşıktır. Oşinografiden roket motorlarına, petrol endüstrisinden astrofiziksel olaylara kadar çok fazlı kararsızlıkların hem doğada hem de endüstride birçok örneği vardır. Tüm bu uygulamalarda geçişin başlangıç noktası bilgisinin edinilmesi çok önemlidir. Bu çalışmada çok fazlı akışların kararsızlığı, özellikle arayüzlerdeki kararsızlıklar üzerinde durulmuştur. Doğrusal kararlılık yaklaşımı kullanılmış ve pertürbasyonların davranışını yakalamak için Orr-Sommerfeld denklemi çözülmüştür. Çok fazlı akış için, her faz için Orr-Sommerfeld denklemleri oluşturulur ve ayrı fazları bağlamak için arayüz koşulları uygulanır. Reynolds sayısı, çok fazlı akışlar için, düzensizlikleri ve kararsızlığı etkileyen boyutsuz tek parametre değildir. Yoğunluk ve viskozite oranları, yüzey geriliminin etkisi, yerçekimi ve zamandan bağımsız hız profillerinin türevlerinin tümü, arayüzdeki kararsızlıklar üzerinde karakteristik etkilere sahip olacaktır. Ayrıklaştırma için bir spektral yöntem, Chebyshev Kollokasyon yöntemi kullanılır. Doğrulama durumları için Mat-

lab, Octave ve C++ programlama dilleri kullanılır. Hem tek fazlı hem de çok fazlı akış için kodların doğrulanması, sayısal sonuçların ve literatürden elde edilen sonuçların karşılaştırılmasıyla elde edilir.

Anahtar Kelimeler: hidrodinamik kararsızlık, çokakışkanlı akışlar, spectral metotlar, özdeğer problemi

to my family

ACKNOWLEDGMENTS

I would like to thank and give my deepest gratitude to my supervisor Professor Hakan I. Tarman. Firstly, he was always there when I needed him and he always helped me to find the right path with his guidance. Secondly, for introducing me to work on a promising and equally thrilling subject.

Especially, I would like to thank my father, Mehmet Çelikkıran and my mother, Filiz Çelikkıran. Their emotional and spiritual support is one of the main power source of mine during this thesis. I hope this will be a cornerstone for our lives.

I would like to acknowledge Roketsan Missiles Inc. and every friend I had in the company who helped me with their support.

I would like to thank Bora Kalpaklı particularly, for his guidance and advice.

TABLE OF CONTENTS

LIST OF TABLES

TABLES

LIST OF FIGURES

FIGURES

LIST OF ABBREVIATIONS

2D	2 Dimensional
3D	3 Dimensional
PDE	Partial Differential Equations
ODE	Ordinary Differential Equations
RTT	Reynolds Transport Theorem
EOS	Equation of State
OS	Orr-Sommerfeld
NS	Navier-Stokes
$\vec{u}$	velocity vector
ρ	density
p	pressure
T	temperature
e	specific internal energy
g	gravitational acceleration
μ	dynamic viscosity
$\vec{\vec{T}}$	stress tensor
$\vec{\vec{\tau}}$	shear stress tensor
Ω	volume of a control volume
$\partial\Omega$	Boundary surfaces of the control volume Ω
$\vec{n}$	unit surface normal vector
R	Reynolds number
Fr	Froude number
We	Weber number
m	Viscosity ratio between two fluids

r	Density ratio between two fluids
n	Height ratio between two fluids
F	inverse Froude number
S	inverse Weber number
$\vec{V}_r$	Relative velocity vector at boundary
$\vec{V}_b$	Boundary velocity vector
$\vec{u}_i$	velocity of interface
φ	Streamfunction
U	Mean velocity profile
ϕ	Amplitude of the perturbation of streamfunction
f	Amplitude of the perturbation of pressure
U'	derivative of U with respect to y coordinate
φ'	derivative of ψ with respect to y coordinate
U_τ	Interfacial Shearing Mean Velocity
σ	Surface tension of interface
η	Deviation of y
N	Amplitude of η
Z	Zero Matrix
I	Identity Matrix
D_i^1	1st Chebyshev Differentiation Matrix of i phase
D_i^2	2nd Chebyshev Differentiation Matrix of i phase
D_i^3	3rd Chebyshev Differentiation Matrix of i phase
D_i^4	4th Chebyshev Differentiation Matrix of i phase
BC	Boundary Condition
IC	Interface Condition
$(PM)_i$	Phase Matrix of i phase
MM	Multiphase Matrix

KHI	Kelvin-Helmholtz Instability
RTI	Rayleigh-Taylor Instability
RMI	Richtmyer-Meshkov Instability

CHAPTER 1

INTRODUCTION

1.1 Two Phase Interface Instabilities

In nature, the instabilities of fluid flow can be observed nearly everywhere. One example is the turbulent flow that is considered to be a result of successive instabilities experienced by a basic laminar flow according to scenarios of transition from laminar to turbulent flow. Turbulent flow is still an unresolved issue for fluid mechanics, and most of the fluid flows encountered in nature, and in engineering applications are turbulent. There is a trade-off between laminar and turbulent flows for their benefit. Depending on the application (physical problem at hand), either can be favorable. To decide and control the flow regime, starting point of the transition from laminar flow to turbulent flow has utmost importance for flow phenomena. If a flow system is considered stable when the regime is laminar, then it is stated as unstable when its regime is turbulent. Any physical phenomenon which leads the flow system to turbulence can be considered as instability. For example, in single-phase flows, the fluid's inertial effects due to convection create instability when they overcome the damping-stabilizing effects such as viscous forces. Acoustic instability can come into play when the flow is compressible. In multi-phase flows, physical effects are multiplied, and the system is more complicated. While inertial and viscous effects still hold their importance for stability, the existence of an interface between flow constituents is an additional physical source for instability. In the text, the term "multi-phase" may also be used to refer to multi-fluid cases for brevity. In particular, the interest in this thesis is in two-phase flows.

For immiscible fluids, the interface can be considered discontinuity where the fluids'

physical variables change abruptly. Like every discontinuity, the interface has to obey physical conservation laws. Therefore, abrupt changes of each side of the interface have to balance each other in terms of conservative variables. From stability point of view, there are two acting effects in play, stabilizing and destabilizing effects. Viscous effects and surface tension can be considered as stabilizing, damping effects. Gravity, inertial forces, and property ratio can be regarded as destabilizing effects. Depending on the physical application, dominant effect of stabilizing and destabilizing forces may differ.

Buoyancy-driven instabilities are dominated by high-density ratio of fluids and gravity. Heavier fluid is placed at the upper part of the lighter fluid. Due to gravity, there is a force at the interface from heavier fluid to lighter fluid. If the surface tension at the interface, as a stabilizer, can not balance the force due to gravity, instability is triggered. Representation of physical mechanism can be observed Figure 1.1. Rayleigh-Taylor Instability and Richtmyer-Meshkov Instability are both Buoyancy-Driven Instabilities. The mechanisms of these two instabilities are similar. The difference is Rayleigh-Taylor is driven by constant acceleration, and Richtmyer-Meshkov is driven by impulsive acceleration.

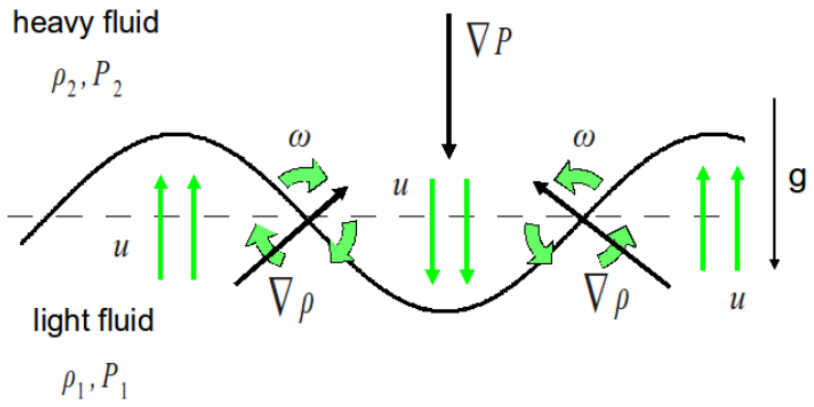

Figure 1.1: Physical effects for the mechanism of Buoyancy-Driven Instabilities[3]

Inversion of a full glass of water is a good real-life example for Rayleigh-Taylor Instability. When the glass is covered with a sheet and inverted, the atmospheric pressure hold the water in place due to fluid statics. Without the sheet cover, however, the

water falls out because air as less dense fluid moves into the water and creates an instability due to the perturbations at the interface forming mushroom-like structures of water at the interface (Figure 1.2). If you, instead, consider a covered straw with water in it, the water stays in place. The diameter of the straw is too small for destabilizing perturbations to occur. In this case, the destabilizing force created by the water as the heavier fluid at the interface due to the density stratification and gravity can be countered by the surface tension. As an extension of this example to demonstrate Richtmyer-Meshkov instability, if the straw is shaken, thus, creating impulsive accelerations, the critical length scale of destabilizing perturbations is lowered enough to make the flow unstable and the water flows out.

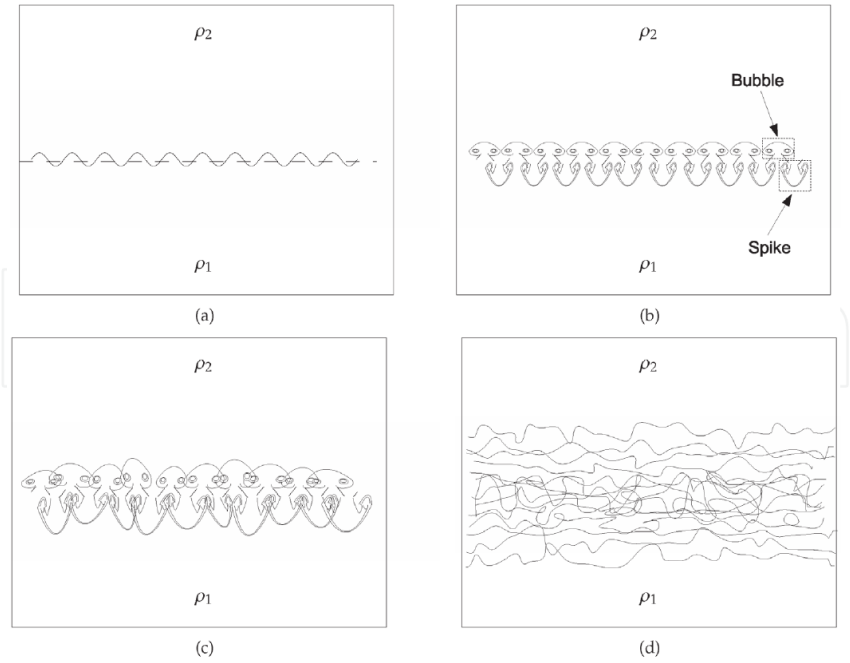

Figure 1.2: Step by step progress of Rayleigh-Taylor Instability [4]

Rayleigh-Taylor instabilities can also be observed in inertial confinement systems. However, the acceleration of the system is impulsive, generally with a shock wave. Therefore, these physical cases are considered as Richtmyer-Meshkov Instabilities. Fusion applications (inertial confinement, magnetized fusion), supernovae, DDT (deflagration to detonation) applications are examples of Richtmyer-Meshkov instability.

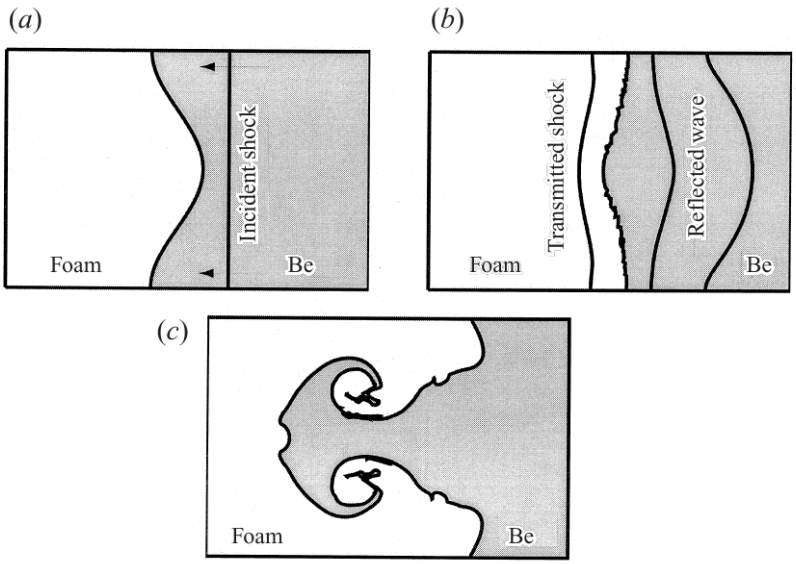

Figure 1.3: Interaction of Shock wave with Interface of multi-phase system generate Richtmyer-Meshkov Instability [5]

Shear-Driven Instabilities are generated by velocity differences between flow constituents. Differences in velocity profile creates different shear stresses at interface. Due to difference in velocity and shear stress, interface will have spatial movement and take the form of sinusoidal wave, effect of pressure will alter at different locations of the wave and normal stress at both sides of interface will change. Visualization of Shear-Driven Instabilities is represented at Figure 1.4.

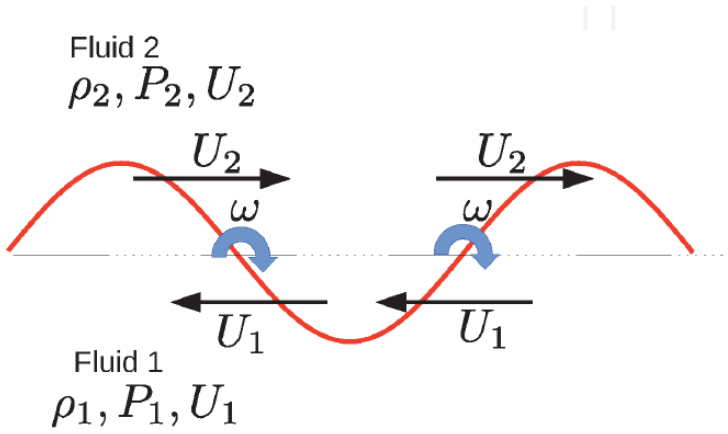

Figure 1.4: Physical effects for the mechanism of Shear-Driven Instabilities [4]

Velocities of both phases can be in parallel direction with different amplitude (Figure 1.5). If the stabilizing forces such as surface tension and gravity (sometimes) can not overcome the destabilizing effect, then instability will start to grow. Growing instabilities will "roll up" as the shearing effect of the faster fluid and altering pressure forces them to close. Entire mechanism of Kelvin-Helmholtz Instability can be observed in Figures 1.5 and 1.6.

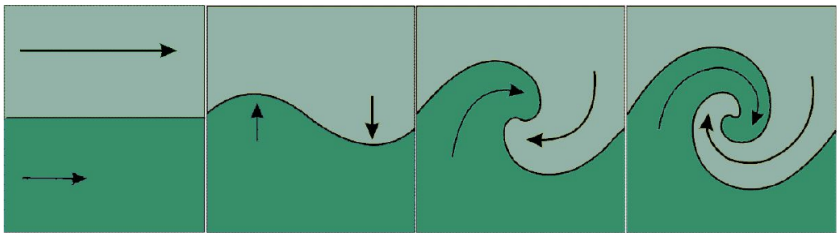

Figure 1.5: Starting of Kelvin-Helmholtz Instability "Roll-up" [6]

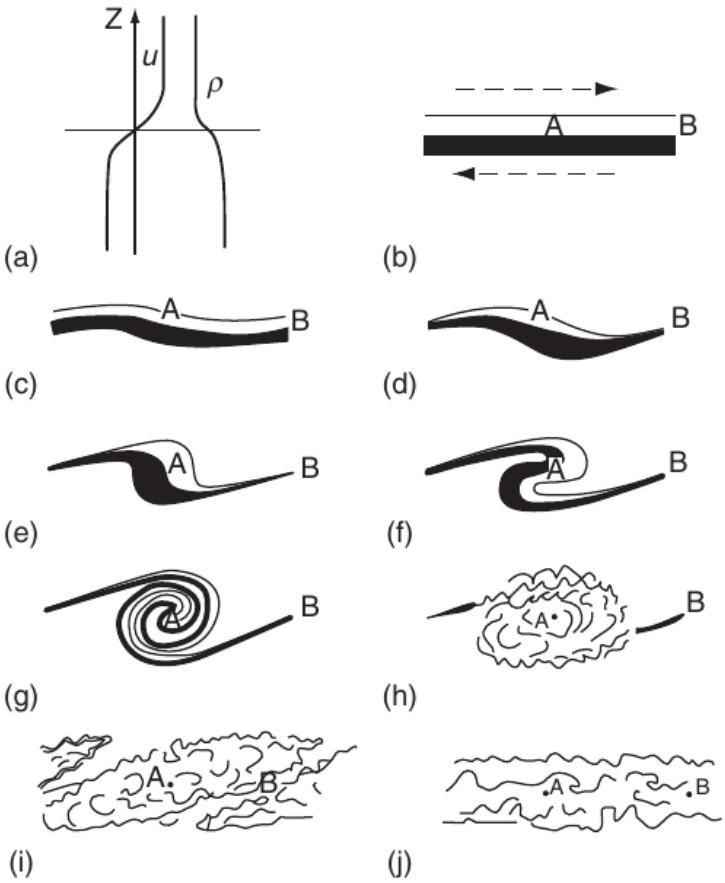

Figure 1.6: Kelvin-Helmholtz Instability Progress and Mechanism [7]

Kelvin-Helmholtz Instability is a famous Shear-Driven flow instability. It can occur in numerous places such as in ocean waves, clouds in atmospheres, at the wake region of airfoils, coronal mass injections in sun. In astrophysical cases, magnetic effects can be included to physics. However, this situation does not alter the "shear-driven" nature of the instability. Two physical examples of Kelvin-Helmholtz Instability can be observed in Figures 1.7 and 1.8.

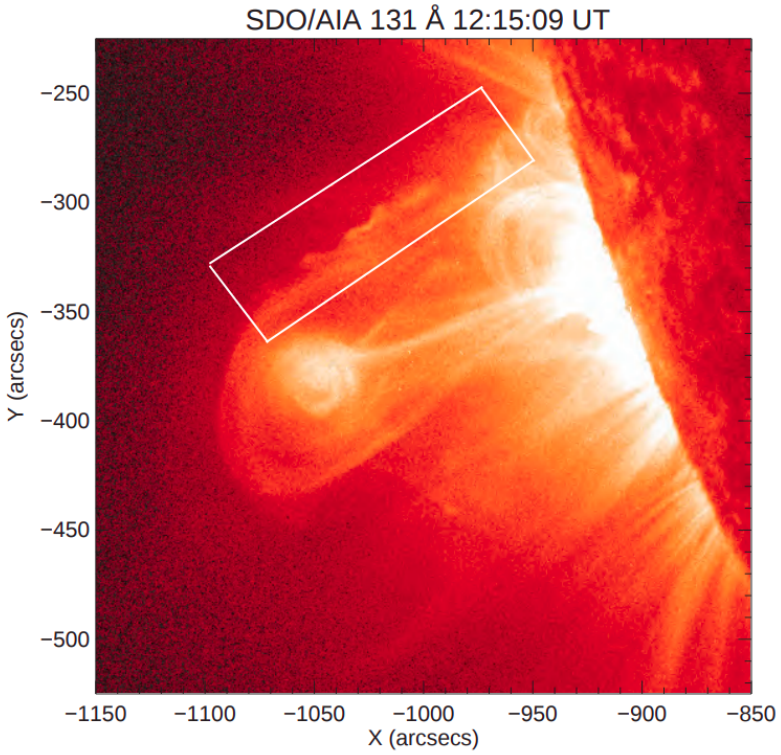

Figure 1.7: A physical example for Kelvin-Helmholtz Instability: Coronal Mass Ejection [8]

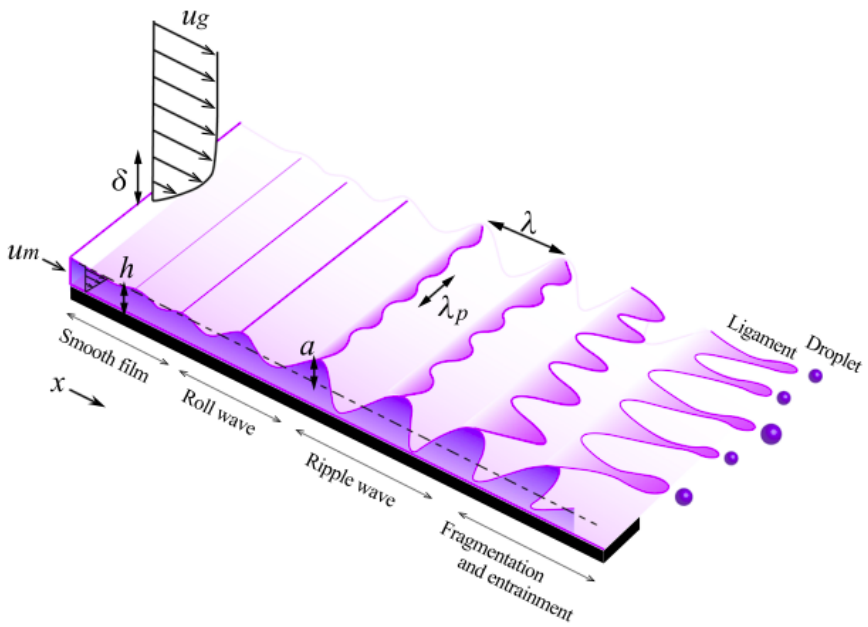

Figure 1.8: Instabilities on liquid film sheared by faster gas leads to entrainment [9]

It has to be noted that depending on geometry and physical case, gravity effect can take the roles of both stabilizing and destabilizing. Imagine the system Figure 1.5, if the system is horizontal as it is stated, then gravity will have stabilizing effect, as it is trying to "damp" the waves. However, if the system is vertical, the gravity will help the shearing effect and will increase the instability. It can even create its own "small scale" Rayleigh-Taylor Instability inside a "large scale" Kelvin-Helmholtz Instability.

As it is mentioned before, physical sources for instabilities in the case of multiphase/-multifluid flows are more numerous than described by the Reynolds number that represents the relative strength of inertial to viscous forces. These physical sources can take the role of stabilizing or destabilizing depending on the physical case. Also, their effects can be coupled to generate complex instabilities. In general, if the flow is starting to become unstable, the instabilities occur at different stages with different levels. However, the amplitudes of the different instability sources are very near to each other, then their effects may be combined.

1.2 Numerical Methods to Capture Interface Instabilities

1.2.1 Linear Hydrodynamic Stability Theory

Linear hydrodynamic stability theory that deals with the evolution of small disturbances in flow. After the disturbances grow, however, the nonlinear stability theory takes over. Both theories can be applied to two-phase flow system similar to single phase flows. For example, Orr-Sommerfeld equation which governs the linear stability of any mean shear flow can be derived for each phases. Interface conditions which are derived from conservation laws at the interface are then applied to connect each individual phase [24][17]. Investigations of inclined plane and free surface flow instabilities are good examples of two-phase applications of linear theory [25]. Generic derivation of interface conditions in terms of perturbation amplitudes is very important. Works of Yih [26], [27], [28], and [29] made important contributions on this matter. Two-phase Poiseuille flow interface conditions are derived including the effects of gravity and surface tension. Main attention is given on the topic of viscosity stratification. Shearing effects are thought to be more important for free surface flows such as sea surface flows under wind shear or liquid film flows. Gas or the lighter fluid which is stationed at the upper part of the system has low density when it is compared to liquid at the lower part. In some cases, upper fluid have higher velocity, thus creating high shear stress at the interface. Viscosity stratification are dominant in these kind of flows. Hooper's works [30], [31] [32] provide effect of different mean velocity profiles on two-phase flow instabilities. Couette and Poiseuille flows are used in viscosity stratification problem. Kelvin-Helmholtz instability is and important example for shearing two phase flows. Viscosity is directly linked to the derivatives of the mean velocity. However, as it is stated in [33], physical effects of viscosity stratification and derivatives of mean velocity profile can be differ from each other. Effect of density stratification is generally observed in heavy fluid reside on the upper part of two-phase system. Due to effect of the gravity heavier fluid forces the interface and if surface tension force is overwhelmed, then Rayleigh-Taylor instability will start. Rayleigh-Taylor instability can trigger more complex instabilities such as Richtmyer–Meshkov instabilities. Physical effects of the instabilities can also be combined if their energy levels are near to each other [33]. It is not always easy to de-

fine the physical effects distinctly. Work of Kelly [34] is illuminating in this manner. Physical effects of the different terms in interface conditions are investigated.

Studies with different numerical methods are conducted in several references [35], [36], [37], [38], [39], [40], [41]. Several methods such as shooting, compound matrix, Chebyshev collocation methods are used for the solution two-phase Orr-Sommerfeld equations. It is observed that due to its high accuracy and easier application for multi-layer flows, Chebyshev collocation method is considered to be one of the best approaches. Domain decomposition method is applied for multi-phase flow with turbulent mean flow velocity profiles [42]. In this study, Boomkamp's method is adopted. Kaffel [22] also used a similar method for simpler two-phase flow problem and the implementation of the algorithm used is explained in detail.

1.2.2 Computational Fluid Dynamics

Rather than using reductive assumptions for linear and nonlinear hydrodynamic theory, whole equation system for multi-phase flow can be solved to acquire the motion of interfaces. This approach is similar to capturing up to Kolmogorov scale eddies in single phase flow which is called Direct Numerical Simulation (DNS). However, similar to single phase flow, capturing interfacial instabilities requires very large number of computational elements and consumes huge amount of computing time. If this computational time can be tolerated, DNS of multi-phase Navier-Stokes solutions with appropriate interface capturing method may reveal full picture about the instabilities. In theory, entire transition can be captured without any restrictions on geometry or flow regime.

High order methods are used in order to decrease the number of computational elements to capture physical phenomenon. However, there is always a trade-off for high order methods. In general, computational time is increased for high order methods because of large number of algebraic operations as well as deteriorating conditioning of the resulting system. High order methods are not generically efficient when it is compared to conventional lower order methods such as finite volume method. Despite this, spectral methods are a common high order method of choice for Navier-Stokes equations in order to capture interface instabilities accurately [43]. Highly

resolving interpolation techniques based on the orthogonal Jacobi polynomials, such as Chebyshev and Legendre polynomials lie at the heart of spectral methods.

Sharpness of the interface creates another issue for the higher order methods. Smoothness is an important criteria for the convergence of high order methods and interface sometimes has to be captured as discontinuity. Smoothness and discontinuity contradicts each other mathematically and application of high order methods create smearing for interface capturing. Resolution or modeling of interface is the utmost importance for multi-phase flows. Different methods are developed in order to capture the interface which can be found at [44] and [45]. Diffuse interface methods are gained attention recently. Rather than considering the interface as a zero-thickness discontinuity, these methods construct a balance between diffusion and sharpness of the interface [46]. This approach allows the method to capture interface sharply when it is needed such as stratified flows and diffuse the interface when multi-phase mixture is modelled.

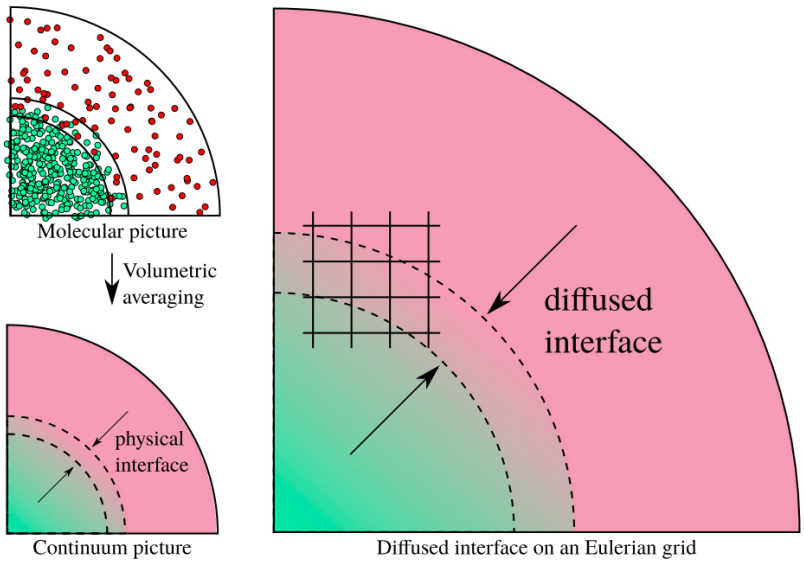

Figure 1.9: Diffuse interface method at the continuuum level [10]

1.2.3 Aim of the Study

The main motivation of this study is to generate a computation code framework for investigation of multi-phase flow instabilities using high-order numerical methods.

Physical and mathematical aspects of this motivation is numerous and they be summarized as follows:

- Generic stability theory for various systems:

  Numerical methods, control systems, and hydrodynamics are some examples. Instability can be expressed as the change from the current state to another, more chaotic state. It is generally used to identify and execute "control" on phenomena. Therefore, its generic understanding and implementation of the physical processes are crucial for conducting hydrodynamic stability investigations.

- Physics of multi-phase flows:

  The physics of transition to turbulence is already very complex, and it is still an active research area. However, it is generally characterized by Reynolds number in hydrodynamic phenomena. In the case of multi-phase flows, such as two fluids with different physical properties (densities, viscosities, etc.) meeting each other at the interface, the existence of the interface creates its own physical effects (e.g. surface tension). The number of physics, thus the source for instabilities, is multiplied. Therefore, understanding the physics of multi-phase flow is an essential part of this study.

- High-order computational approach (Spectral methods):

  By the nature of the problem, investigating hydrodynamic instabilities requires high accuracy. Spectral methods are global methods that are perfect for boundary value problems. Use of orthogonal basis functions and their powerful numerical approximation of differentiation operations are crucial in capturing instabilities accurately.

CHAPTER 2

SINGLE PHASE FLOW STABILITY

2.1 Stability Analysis

2.1.1 Generic Stability definition

The immunity level of a dynamical system to small disturbances can be identified as stability of a system [47]. Definition of stability comes from the reaction of a system to a disturbance. If the system is decreasing the amplitude of the disturbance, then the system can be called "stable". However, if the disturbance's amplitude is increasing, the reaction of the system can be called unstable. A better explanation will come from the amplitudes of the disturbances. An important criterion is starting and finishing amplitudes of the disturbances:

- If a disturbance with an infinitesimal amplitude is applied to the system and the system does not magnify this initial amplitude, then the system is considered to be "stable".

- If a disturbance with an infinitesimal amplitude is applied to the system and the system magnifies this initial amplitude that reaches to a finite value, then the system is considered to be "unstable".

The behavior of the amplitude of the infinitesimal disturbance can be observed in different system states in Figure 2.1.

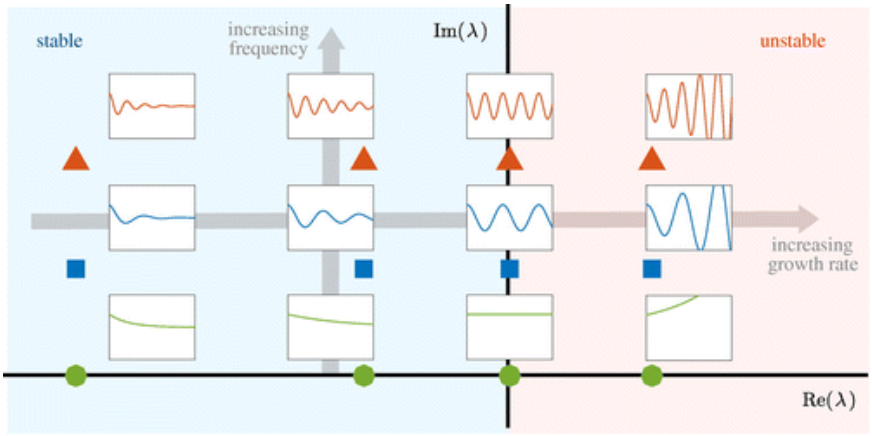

Figure 2.1: Stability of a system: Stable, Marginally Stable, Unstable [11]

2.1.2 Stability definition for Fluid Flows

The main difference between stable and unstable states of the fluid flow is the nature of alterations of the mean flow. If these changes are reversible, which means, if the mean flow can return to its initial state as time passes, the flow can be considered "stable". However, if these alterations are irreversible, which means, the disturbances have effect on the definition of the mean flow and return to previous initial state can not be possible anymore as time progresses, the flow is considered as "unstable" [47]. Transition from laminar to turbulent flow is conceptualized to be as a result of such irreversible alterations to intermediate flow regimes caused by the disturbances ever present in the environment. Each of these alterations introduce new flow regimes that have smaller time and space scales that are referred to as eddies or swirls as represented in Figure 2.2.

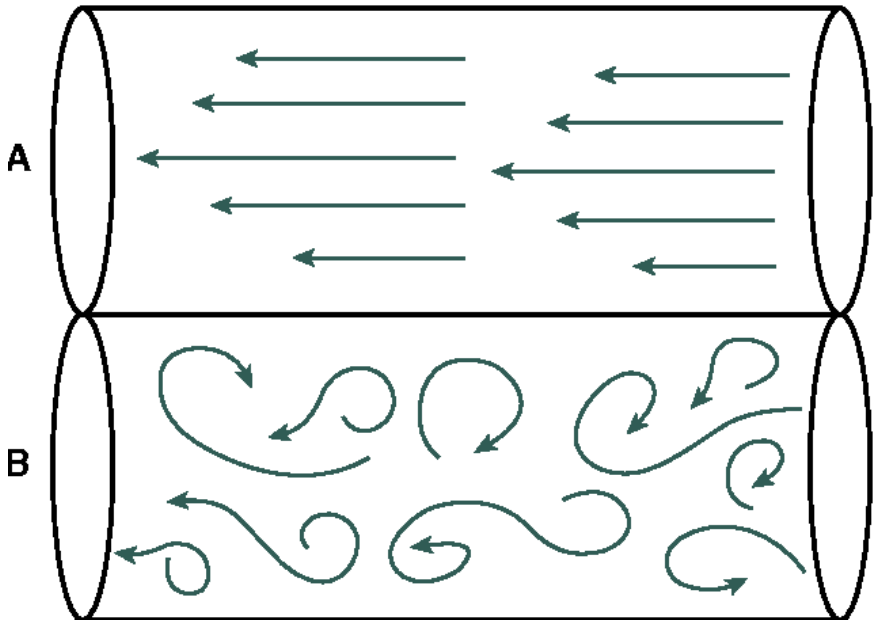

Figure 2.2: Nature of Laminar (A) vs Turbulent Flows (B) [12]

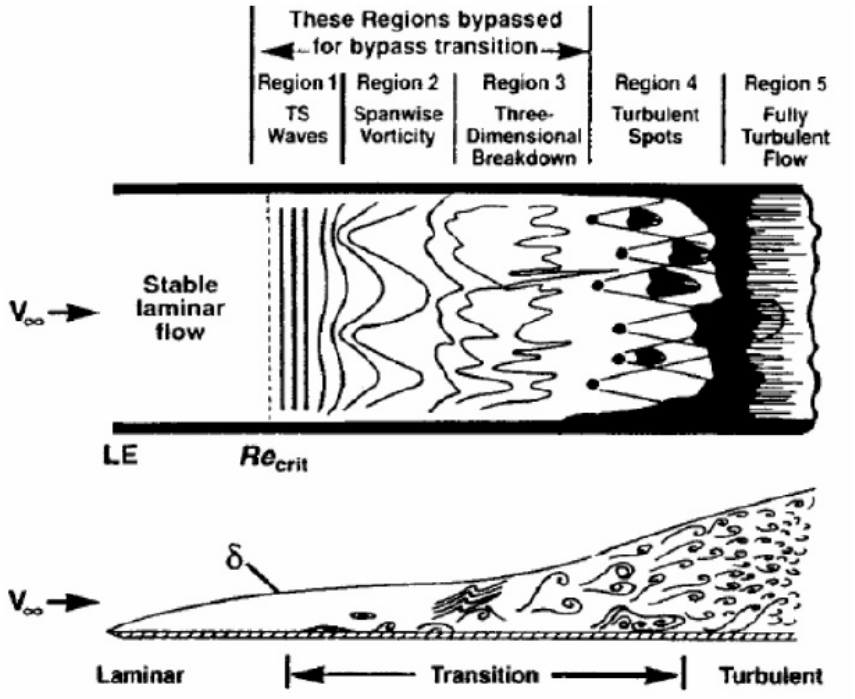

Figure 2.3: Nature of Laminar (A) vs Turbulent Flows (B) [13]

2.1.3 Stability analysis with Perturbation in Fluid Flow

2.1.3.1 Normal Modes

In linear hydrodynamic theory, first, mean (time-independent) velocity and pressure fields are perturbed, then due to linearity assumption, nonlinear effects are neglected. Subsequently, the *normal modes* method can be applied to represent the linear behavior of perturbations.

In the normal modes method, perturbations are modeled as superposition of sinusoidal waves that is allowed by the linearity assumption of the perturbation equation. The time-independence of the mean flow leads to a linear perturbation equation with time independent coefficients and so a generic perturbation flow variable $v(x, y, z, t)$ can be written in the form of normal modes [48]

$$v\left(x, y, z, t\right) = \tilde{v}\left(x, y, z\right) e^{-i\omega t}$$

where $\tilde{v}\left(x, y, z\right)$ is the amplitude, ω is referred to as the eigenvalue and its imaginary part characterizes temporal stability. For parallel flows, say, the mean flow is only a function of the spatial variables y, then the perturbation can be represented in the form

$$v\left(x, y, z, t\right) = \tilde{v}\left(y\right) e^{i(\alpha x + \gamma z - \omega t)}. \tag{2.1}$$

This is actually Fourier representation for the perturbation where the term $e^{i(\alpha x+\gamma z-\omega t)}$ is a basis for Fourier expansion with the wave numbers α and γ. $\tilde{v}\left(y\right)$ is the amplitude of the perturbation.

The stability analysis based on monitoring the temporal evolution of the individual normal modes in the representation of the perturbation breaks down when the linearity assumption looses its validity. In that case, the evolution of the individual normal modes starts to effect each other and they become correlated.

2.1.3.2 Squire's Theorem

Squire's Theorem states that for parallel flows, every 3D disturbance has a corresponding 2D disturbance which is more unstable. Therefore, 2D investigation is

enough to capture most unstable disturbance inside the flow [1] [49]. It may be mathematically represented in the form

$$Re_{2D} = \frac{\alpha Re_{3D}}{\sqrt{\alpha^2 + \gamma^2}} = \frac{\alpha}{\tilde{\alpha}} Re_{3D} = Re_{3D} cos(\phi) \tag{2.2}$$

where Re stands for the Reynolds number. Squire's Theorem simplifies the mathematical analysis for the system and allows simplified form of representation using only the perturbation of the form, $\tilde{v}\,(y)\, e^{i(\alpha x - \omega t)}$. However, it can be only applied to parallel flows in which the mean velocity does not vary in the direction of the flow. In other flow configurations, a 3D disturbance analysis has to be performed to determine the stability of the flow [29] [47] .

2.1.3.3 Temporal Stability

For temporal stability, spatial wave number α is considered to be real and investigation of the instability is performed in the time domain. The perturbation flow variable can then be written as

$$\begin{aligned} v\,(x, y, t) &= \tilde{v}\,(y)\, e^{i(\alpha x - \omega t)} \\ &= \tilde{v}\,(y)\, e^{i(\alpha x - \omega_r t - i\omega_i t)} \\ &= \tilde{v}\,(y)\, e^{i\alpha(x - c_r t - i c_i t)} \\ &= \tilde{v}\,(y)\, e^{\alpha c_i t} e^{i\alpha(x - c_r t)} \end{aligned} \tag{2.3}$$

where $\omega = \omega_r + i\omega_i = \alpha\,(c_r + i c_i)$. Complex exponential part of (2.3) is oscillatory and has magnitude of unity. Thus, it has no effect on the stability considerations. However, the real exponential part together with $\tilde{v}\,(y)$ determines the amplitude of the perturbation. Therefore, c_i becomes the criteria for the temporal stability [50]

$$e^{\alpha c_i t} = \begin{cases} \infty \rightarrow \text{growth}, & \text{if } c_i > 0, \\ 0 \rightarrow \text{decay}, & \text{if } c_i < 0. \end{cases} \tag{2.4}$$

2.1.3.4 Spatial Stability

For spatial stability, spatial wave number α is considered to be complex while ω is taken as real. The perturbation flow variable can then be written as

$$\begin{aligned} v\left(x,y,t\right) &= \tilde{v}\left(y\right)e^{i(\alpha x-\omega t)} \\ &= \tilde{v}\left(y\right)e^{i(\alpha_r x+i\alpha_i x-\omega t)} \\ &= \tilde{v}\left(y\right)e^{i\omega(k_r x+ik_i x-t)} \\ &= \tilde{v}\left(y\right)e^{-\omega k_i x}e^{i\omega(k_r x-t)} \end{aligned} \tag{2.5}$$

Similar to (2.3), the complex exponential part of (2.5) does not contribute to the amplitude. However, the real exponential part of (2.5) when multiplied by $\tilde{v}\left(y\right)$ is the amplitude of the perturbation. Therefore, as it can be observed in (2.6), the signature of k_i becomes the criteria for the spatial stability [50]

$$e^{-\omega k_i x} = \begin{cases} \infty \rightarrow \text{growth}, & \text{if } k_i < 0, \\ 0 \rightarrow \text{decay} & \text{if } k_i > 0. \end{cases} \tag{2.6}$$

2.1.4 Derivation of Orr-Sommerfeld (OS) Equation [1]

2.1.4.1 Assumptions

- Incompressible Fluid Flow:

$$\rho = constant \tag{2.7}$$

(2.7) is also an Equation of State (EOS) for the incompressible flows. With this assumption, conservation of mass equation (3.3) in differentiable form becomes:

$$\nabla.\vec{u} = 0. \tag{2.8}$$

It is also called divergence-free condition. This equation is not a transport equation for density anymore. It becomes a restriction on the velocity vector. This nature of the equation has both advantages and disadvantages. It is very useful for the simplification of some terms in the governing differential model for incompressible flows.

- 2D Flow Domain:

  If the underlying mean flow has parallel flow character, then Squire's Theorem justifies the use of 2D flow geometry without loss of generality. The associated differential model is

$$\rho\left(\frac{\partial u}{\partial t}+u\frac{\partial u}{\partial x}+v\frac{\partial u}{\partial y}\right)=-\frac{\partial P}{\partial x}+\mu\left(\frac{\partial^2 u}{\partial x^2}+\frac{\partial^2 u}{\partial y^2}\right), \tag{2.9a}$$

$$\rho\left(\frac{\partial v}{\partial t}+u\frac{\partial v}{\partial x}+v\frac{\partial v}{\partial y}\right)=-\frac{\partial P}{\partial y}+\mu\left(\frac{\partial^2 v}{\partial x^2}+\frac{\partial^2 v}{\partial y^2}\right). \tag{2.9b}$$

  These are Navier-Stokes (NS) equations which are the 2D incompressible version of conservation of momentum equation (3.4).

  Energy conservation equation (3.5) is decoupled from mass and momentum conservation equation due to incompressibility assumption. Coupling between thermodynamic and mechanic variables inside the flow domain does not exist or is very weak for incompressible flows. Equation of State (2.7) does not connect thermodynamic variables. Coupling between pressure and density does not exist, so pressure work can not be done due to zero change in volume. In general, the pressure variable P in the fluid flows has dual physical purpose. It has both thermodynamical and mechanical roles inside the flow domain. However, when the incompressibility assumption is made, pressure has only mechanical nature inside the flow domain. In this work, only hydrodynamic instability is investigated. Therefore, energy conservation equation will not be used.

- Unidirectional Mean (Primary) Flow:

$$\vec{U}=U(x,y)\,\vec{e}_x \tag{2.10}$$

  where $\vec{e}_x$ is the unit vector along x direction. In 2D flow geometry, together with the divergence-free condition, it implies that $U=U(y)$, that is unidirectional mean flow has the parallel flow property in 2D geometry. Its physical interpretation is that the main effect of the Mean Velocity Profile on the flow is the *shearing effect*.

2.1.4.2 Non-dimensionalization of Navier-Stokes Equations

By using L to denote the length scale and U_∞ for the velocity scale, and consequently L/U_∞ for time and ρU_∞^2 for pressure, non-dimensional form of the NS equations becomes

$$\frac{\partial u_i}{\partial t} + u_j \frac{\partial u_i}{\partial x_j} = -\frac{\partial P}{\partial x_i} + \frac{1}{Re}\frac{\partial^2 u_i}{\partial x_j \partial x_j} \tag{2.11}$$

where Einstein index summation convention is used. For convenience, the same notation for both dimensional and non-dimensional flow variables are used. Thus, under the absence of other external physical effects, the whole flow regime is characterized by a single non-dimensional parameter, namely the Reynolds number, $Re = \rho U_\infty L/\mu$. It, in fact, represents the relative strength of inertial versus viscous forces.

2.1.4.3 Linear Perturbation Equations

First, the dependent flow variables are split into the mean and perturbation components

$$\vec{u}(x,y,t) = U(y)\vec{e}_x + \vec{u}\,'(x,y,t) \tag{2.12a}$$

$$p(x,y,t) = P(x,y) + p'(x,y,t) \tag{2.12b}$$

and then they are substituted into the NS equations (2.11) to get

$$\frac{\partial u_i'}{\partial t} + \left(U\delta_{1j} + u_j'\right)\frac{\partial\left(U\delta_{1i} + u_i'\right)}{\partial x_j} = -\frac{\partial\left(P + p'\right)}{\partial x_i} + \frac{1}{Re}\frac{\partial^2\left(U\delta_{1i} + u_i'\right)}{\partial x_j \partial x_j} \tag{2.13}$$

where δ_{ij} denotes the Kronecker delta. Mean flow variables also satisfy the NS equations

$$0 = -\frac{\partial P}{\partial x} + \frac{1}{Re}\frac{d^2 U}{dy^2} \qquad \text{and} \qquad 0 = -\frac{\partial P}{\partial y} \tag{2.14}$$

that are subtracted from (2.13) to yield the perturbation equations

$$\frac{\partial u_i}{\partial t} + U\delta_{1j}\frac{\partial u_i}{\partial x_j} + u_j\frac{dU}{dx_j}\delta_{1i} + u_j\frac{\partial u_i}{\partial x_j} = -\frac{\partial p}{\partial x_i} + \frac{1}{Re}\frac{\partial^2 u_i}{\partial x_j \partial x_j}. \tag{2.15}$$

Here and in the rest of the thesis, the primes over the perturbation variables will be removed for notational convenience. They are then linearized based on the (additional)

assumption of smallness of the perturbations in magnitude that yields the linear perturbation equations

$$\frac{\partial u}{\partial t} + U\frac{\partial u}{\partial x} + v\frac{dU}{dy} = -\frac{\partial p}{\partial x} + \frac{1}{Re}\left(\frac{\partial^2 u}{\partial x^2} + \frac{\partial^2 u}{\partial y^2}\right) \tag{2.16a}$$

$$\frac{\partial v}{\partial t} + U\frac{\partial v}{\partial x} = -\frac{\partial p}{\partial y} + \frac{1}{Re}\left(\frac{\partial^2 v}{\partial x^2} + \frac{\partial^2 v}{\partial y^2}\right) \tag{2.16b}$$

2.1.4.4 Streamfunction Equation

In order to remove pressure gradients, the y-derivative of (2.16a) is subtracted from the x-derivative of (2.16b) with a cost of increased order of derivatives, to get

$$\frac{\partial}{\partial t}\left(\frac{\partial u}{\partial y} - \frac{\partial v}{\partial x}\right) + \frac{\partial}{\partial y}\left(U\frac{\partial u}{\partial x}\right) - \frac{\partial}{\partial x}\left(U\frac{\partial v}{\partial x}\right) + \frac{\partial}{\partial y}\left(v\frac{dU}{dy}\right) = \frac{1}{Re}\left(\frac{\partial^3 u}{\partial y^3} - \frac{\partial^3 v}{\partial x^3} + \frac{\partial^2}{\partial x \partial y}\left(\frac{\partial u}{\partial x} - \frac{\partial v}{\partial y}\right)\right). \tag{2.17}$$

This equation can further be simplified by introducing streamfunction φ defined by

$$u = \frac{\partial \varphi}{\partial y} \qquad \text{and} \qquad v = -\frac{\partial \varphi}{\partial x} \tag{2.18}$$

that is commonly used in incompressible flows and the formulation of the velocity field in terms of the streamfunction (2.18) enforces the divergence-free character of the velocity field. The introduction of the streamfunction into (2.17) reduces the number of unknowns to one with a mathematical cost of further increase in the order of derivatives by one. The resulting streamfunction equation is

$$\frac{\partial\left(\nabla^2\varphi\right)}{\partial t} + U\frac{\partial\left(\nabla^2\varphi\right)}{\partial x} - \frac{d^2U}{dy^2}\frac{\partial\varphi}{\partial x} = \frac{1}{Re}\left(\frac{\partial^4\varphi}{\partial x^4} + 2\frac{\partial^4\varphi}{\partial x^2\partial y^2} + \frac{\partial^4\varphi}{\partial y^4}\right) \tag{2.19}$$

where $\nabla^2\varphi = \partial^2\varphi/\partial x^2 + \partial^2\varphi/\partial y^2$. When the normal modes representation of the perturbation streamfunction

$$\varphi(x, y, t) = \phi(y)e^{i\alpha(x-ct)} \tag{2.20}$$

in terms of the phase speed c and streamwise wave speed α is introduced into (2.19), it yields the Orr-Sommerfeld Equation:

$$\phi'''' - 2\alpha^2\phi + \alpha^4\phi = i\alpha Re\left((U-c)\left(\phi'' - \alpha^2\phi\right) - \phi U''\right) \tag{2.21}$$

Orr-Sommerfeld Equation is a an Ordinary Differential Equation (ODE) and it is obtained from the Navier-Stokes equations which are Partial Differential Equations (2.11) by linearization first and subsequently separation of variables and the normal modes representation. Furthermore, it represents a differential *eigenproblem* for both c (for temporal stability) and α (for spatial stability). If the spatial stability approach is chosen, Orr-Sommerfeld Equation becomes a nonlinear differential eigenproblem with α as the eigenvalue. On the other hand, if the temporal stability approach is chosen, Orr-Sommerfeld Equation becomes a linear differential eigenproblem with c as the eigenvalue. The dispersion relation of single phase Orr-Sommerfeld equation is symbolically represented by

$$c = c\,(Re, \alpha) \tag{2.22}$$

2.2 Numerical Method of Solving Orr-Sommerfeld Equation

Orr-Sommerfeld equation in this context is considered as an eigenvalue problem. However, it is also an ODE. Therefore, numerical methods for solving ODEs can be applied to solve it. In this thesis, a Spectral method is used to discretize the Orr-Sommerfeld equation and reduce it to an algebraic eigenvalue problem.

2.2.1 Why Spectral Methods?

The main reason for the choice of Spectral methods is their deliverance high accuracy. Study of hydrodynamic stability is a numerically delicate problem as much as it is physically so. Computational instabilities may arise when using low order conventional methods and contaminate the numerical results. Spectral methods are generally numerically stable and highly accurate. In fact, under the condition of smoothness of the underlying mathematical problem, Spectral methods achieve exponential (geometric) order of accuracy in comparison to conventional methods that provide only an algebraic order of accuracy as compared in Figure (2.4).

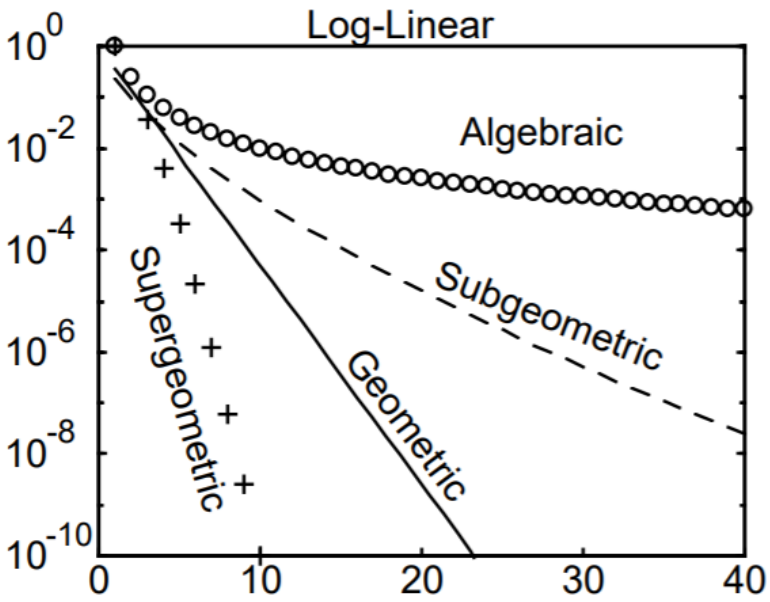

Figure 2.4: Error vs number of points. Comparison of different convergence characteristics of decreasing errors [14]

Another advantage of the Spectral methods is its global nature as depicted in Figure (2.5) and it is important for the differential eigenproblem at hand that is also a Boundary Value Problem (BVP).

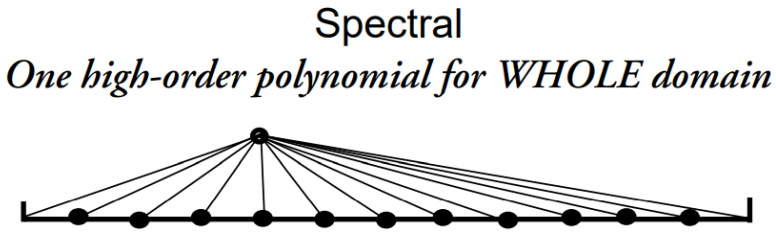

Figure 2.5: Entire domain is represented by single polynomial [14]

2.2.2 Preliminary Concepts

Spectral methods are numerical methods which are mainly used to solve differential and integral equations. Main ingredients of these methods are listed below:

- Discretization:

In Spectral methods, the unknown solution $u(x)$ of a differential or integral equation is approximated by a truncated series expansion in terms of some other "known" and "nice" (basis) functions $\phi_n(x)$:

$$u(x) \cong u_N(x) = \sum_{n=0}^{N} a_n \phi_n(x) \tag{2.23}$$

where a_n are the unknown expansion coefficients and N is the order of truncation that amounts to a discrete representation of the unknown function $u(x)$. This truncated representation $u_N(x)$ is then substituted into the differential or integral equation that is symbolically written by

$$\mathcal{L}\{u(x)\} = f(x) \tag{2.24}$$

where $\mathcal{L}$ denotes the differential or integral operator and f is the nonhomogeneous forcing term. This results in a residue (Res) of the approximation

$$Res = \mathcal{L}\{u_N(x)\} - f(x). \tag{2.25}$$

In turn, this residual is minimized in some sense in order to achieve high accuracy in satisfying the differential or integral equation. The handling of the residual and the choice of the basis functions characterize a Spectral method.

- Basis Functions:

  There are certain properties of the basis functions $\phi_n(x)$ that make them "nice" functions [14]. These properties are:

  (i) Numerical Efficiency of the Representation:

  The representation in (2.23) connects the the real (physical) space where the function $u_N(x)$ lives and the *modal* space where the coefficients a_n lives. In the numerical solution procedure, fast and efficient connection between these two spaces is an important factor in the numerical efficiency of the representation.

  (ii) Fast Convergence:

  The order of truncation N required to achieve a desired accuracy (measured in some sense) in representing the actual function $u(x)$ by its truncated representation $u_N(x)$ directly effects the computational labor in the numerical solution procedure. As N increases so does the dimension of the modal space. This

is connected with the degree of smoothness (differentibility) of the solution function space as well as the *resolving power* of the basis functions.

(iii) Completeness:

This entails the ability of the bases to represent of any kind of function in the solution function space to arbitrarily high accuracy when the truncated series expansion have sufficient number of basis functions to represent the function. This also includes the suitability of the basis functions in representing the character of the solution function space such as boundary conditions, periodicity, etc..

(iv) Orthogonality:

The orthogonality of the basis functions with respect to a predefined inner product ensures the linear independence and each carrying an independent character in an hierarchical manner. The orthogonality also contributes to establish a fast and efficient connection between the modal and physical spaces. Generally, orthogonal basis functions are acquired as eigenfunctions of a Sturm-Liouville problem.

2.2.3 Chebyshev Pseudospectral Method

It is an interpolation based Spectral method that uses Chebyshev polynomials $T_n(x)$ as basis functions. They are polynomial solutions to a singluar Sturm-Liouville differential eigenvalue problem and defined by

$$T_n(x) = cos(n\theta) \qquad \text{where} \qquad x = cos(\theta), \tag{2.26}$$

for each integer $n \geq 0$. They are in fact polynomials disguised as trigonometric functions [51],

$$\begin{aligned}
&T_0(x) = cos(0) = 1,\\
&T_1(x) = cos(\theta) = x,\\
&T_2(x) = cos(2\theta) = 2cos^2(\theta) - 1 = 2x^2 - 1,\\
&T_3(x) = cos(3\theta) = 4cos^3(\theta) - 3cos(\theta) = 4x^3 - 3x, ...
\end{aligned}$$

As it follows from (2.26), the Chebyshev polynomials are defined in the interval $-1 \leq x \leq 1$ and bounded $\mid T_n(x) \mid \leq 1$. A desirable property of Chebyshev polynomials is that they satisfy the orthogonality relation defined by the inner product operation

$$\langle\, T_n(x)\,,\, T_m(x)\,\rangle \equiv \int_{-1}^{1} T_n(x)\, T_m(x) \frac{1}{\sqrt{1-x^2}} dx = \gamma_n \delta_{nm}, \tag{2.27}$$

where $\sqrt{\gamma_n}$ is referred to as norm of $T_n(x)$. The orthogonality property (2.27) provides the means to determine the expansion coefficients a_n in the truncated representation

$$u(x) \cong u_N(x) = \sum_{n=0}^{N} a_n T_n(x) \tag{2.28}$$

by using the integral formula

$$a_n = \frac{\langle\, u(x)\,,\, T_n(x)\,\rangle}{\langle\, T_n(x)\,,\, T_n(x)\,\rangle} = \frac{1}{\gamma_n} \int_{-1}^{1} u(x) T_n(x) \frac{1}{\sqrt{1-x^2}} dx. \tag{2.29}$$

Another important property is that the quantity

$$\max_{-1 \leq x \leq 1} \left| u(x) - \sum_{n=0}^{N} a_n T_n(x) \right| \tag{2.30}$$

is a minimum amongst all possible N^{th} degree polynomial representations of $u(x)$ in the form of (2.28). This is called the minimax property of the Chebyshev polynomials.

The evaluation of the expansion coefficients a_n using the integral formula (2.29) is computationally impractical for general functions $u(x)$. The discrete orthogonality property of the Chebyshev polynomials provides the practical resolution of this problem. It is defined by the discrete inner product operation [52]

$$[\, T_n\,,\, T_m\,] \equiv \sum_{j=0}^{N} T_n(x_j) T_m(x_j) \omega_j = \lambda_n \delta_{nm} \tag{2.31}$$

where x_j and ω_j are the Chebyshev Gauss-Lobatto quadrature points and weights, respectively. The quadrature points are the roots of the polynomial $q(x)$ of degree $(N+1)$:

$$q(x) = T_{N+1}(x) - T_{N-1}(x) = -\frac{2}{N}(1-x^2)\frac{d}{dx} T_N(x),$$

given by

$$x_j = -cos\left(\frac{\pi j}{N}\right), \qquad j = 0, ..., N, \tag{2.32}$$

that are also called Chebyshev points. The quadrature weights are given by

$$\omega_j = \begin{cases} \pi/2N, & j = 0, N, \\ \pi/N, & j = 1, ..., N-1. \end{cases} \tag{2.33}$$

For a given function $u(x)$ in $-1 \leq x \leq 1$, using the discrete orthogonality (2.31), we can compute the coefficients

$$b_n = \frac{1}{\lambda_n} \sum_{j=0}^{N} u(x_j) T_n(x_j) \omega_j, \tag{2.34}$$

that when they are used to construct the *modal* expansion

$$u_N(x) = \sum_{n=0}^{N} b_n T_n(x), \tag{2.35}$$

it yields the property $u(x_j) = u_N(x_j)$ that is called the interpolation condition. This can be used to construct *nodal* form of the representation (2.35) as follows

$$\begin{aligned} u_N(x) &= \sum_{n=0}^{N} b_n T_n(x) \\ &= \sum_{n=0}^{N} \left(\frac{1}{\lambda_n} \sum_{j=0}^{N} u(x_j) T_n(x_j) \omega_j \right) T_n(x) \\ &= \sum_{j=0}^{N} u(x_j) \underbrace{\left(\omega_j \sum_{n=0}^{N} \frac{1}{\lambda_n} T_n(x) T_n(x_j) \right)}_{L_j(x)}. \end{aligned} \tag{2.36}$$

The functions $L_j(x)$ are N^{th} degree polynomials called the interpolating Lagrange polynomials that satisfy the cardinality property $L_j(x_k) = \delta_{jk}$. They can also be written in more familiar explicit form

$$L_j(x) = \prod_{\substack{k=0 \\ k \neq j}}^{N} \frac{(x - x_k)}{(x_j - x_k)}. \tag{2.37}$$

The interpolation condition $u(x_j) = u_N(x_j)$ actually implies by (2.35) that

$$u(x_j) - \sum_{n=0}^{N} b_n T_n(x_j) = 0. \tag{2.38}$$

This now gives the means to discretize the symbolic differential or integral equation (2.24), by setting the residue to zero at the Chebyshev (collocation) points x_j

$$Res(x_j) = \mathcal{L}\left\{u_N(x)\right\}|_{x_j} - f(x_j) = 0 \tag{2.39}$$

for $j = 0, ..., N$. This gives $(N+1)$ equations to determine the $(N+1)$ modal coefficients b_n in (2.35) and in turn $u(x_j)$. This is the outline of Chebyshev Pseudospectral Method for solving differential or integral equations.

The nodal representation (2.36) also provides a convenient discrete representation of the derivative operator as follows:

$$\left(\frac{du}{dx}\right)\Bigg|_{x_i} \cong \left(\frac{du_N}{dx}\right)\Bigg|_{x_i} = \sum_{j=0}^{N} u(x_j)\left(\frac{dL_j}{dx}\right)\Bigg|_{x_i}, \tag{2.40}$$

or in matrix form $W = D * U$ where

$$D = \begin{bmatrix} L_0'(x_0) & L_1'(x_0) & \dots & L_N'(x_0) \\ L_0'(x_1) & L_1'(x_1) & \dots & L_N'(x_1) \\ \vdots & \vdots & \ddots & \vdots \\ L_0'(x_N) & L_1'(x_N) & \dots & L_N'(x_N) \end{bmatrix}, \tag{2.41}$$

while

$$W = [\, u_N'(x_0) \quad u_N'(x_1) \quad \dots \quad u_N'(x_N) \,]^T,$$

and

$$U = [\, u(x_0) \quad u(x_1) \quad \dots \quad u(x_N) \,]^T.$$

Here D is called the Chebyshev Differentiation Matrix. Similarly, higher order derivative matrices can be constructed, such as,

$$D^{(2)} = \begin{bmatrix} L_0''(x_0) & L_1''(x_0) & \dots & L_N''(x_0) \\ L_0''(x_1) & L_1''(x_1) & \dots & L_N''(x_1) \\ \vdots & \vdots & \ddots & \vdots \\ L_0''(x_N) & L_1''(x_N) & \dots & L_N''(x_N) \end{bmatrix}.$$

In fact, for Chebyshev polynomial basis, $D^{(2)} = D * D = D^2$. The differentiation matrices are of size $(N+1)$ and rank deficient as much as its order, for example, *rank*$(D) = N$ and *rank*$(D^{(2)}) = N - 1$. This means that in order to remove the rank deficiency, as many additional conditions as the order of the derivative that the differentiation matrix represents, should be supplied. This actually corresponds to the familiar requirement of supplying sufficient number of external (boundary and/or initial) conditions to have a well-posed differential equation.

2.2.4 Numerical Implementation for OS Equations

The collocation discretization (2.40) and the concept of the differentiation matrix (2.41) facilitate a modular construction of a numerical implementation of the Chebyshev Pseudospectral Method to solve the differential equation of interest, namely, Orr-Sommerfeld equation (2.21). As mentioned above, this requires the completion of the problem as a well-posed BVP with appropriate boundary conditions.

The no-slip and rigid wall conditions

$$u|_{\text{wall}} = v|_{\text{wall}} = 0$$

for flow of viscous fluid bounded by a stationary rigid wall provide the required boundary conditions for the OS equations. These, in terms of the streamfunction formulation (2.18) and (2.20), translate into

$$\phi(\pm 1) = \phi'(\pm 1) = 0 \tag{2.42}$$

for two rigid walls located, say, at $y = \pm 1$.

In order to implement the Chebyshev Pseudospectral Method, the computational domain $-1 \leq y \leq 1$ is discretized first, using the Chebyshev points

$$y_j = -cos\left(\frac{\pi j}{N}\right), \qquad j = 0, ..., N. \tag{2.43}$$

The corresponding polynomial representation is

$$\phi(y) \cong \phi_N(y) = \sum_{j=0}^{N} \phi(y_j) L_j(y), \tag{2.44}$$

and we can define the grid function

$$\Phi = [\, \phi_0 \quad \phi_1 \quad \dots \quad \phi_N \,]^T \tag{2.45}$$

where $\phi_j = \phi(y_j)$. The boundary conditions may be implemented as additional conditions

$$\begin{aligned}
\phi(-1) = 0 \quad &\rightarrow \quad \phi_0 = 0, \\
\phi'(-1) = 0 \quad &\rightarrow \quad D_{00}\,\phi_0 + D_{01}\,\phi_1 + \cdots + D_{0N}\,\phi_N = 0, \\
\phi(1) = 0 \quad &\rightarrow \quad \phi_N = 0, \\
\phi'(1) = 0 \quad &\rightarrow \quad D_{N0}\,\phi_0 + D_{N1}\,\phi_1 + \cdots + D_{NN}\,\phi_N = 0,
\end{aligned}$$

where $D_{ij} = L_j'(y_i)$.

Or they may be built in the interpolation polynomials by defining [53],

$$\phi_N(y) = (1 - y^2)q(y), \tag{2.46}$$

where $q(y)$ is a polynomial of degree $\leq (N-1)$ with $q(\pm 1) = 0$ so that $\phi_N(y)$ is a polynomial of degree $\leq (N+1)$ with $\phi(\pm 1) = \phi'(\pm 1) = 0$. The conditions $q(\pm 1) = 0$ can easily be implemented in the corresponding differentiation matrices $D^{(\nu)}$ by removing its first and last rows and columns that the resulting differentiation matrix will be denoted by the notation $\tilde{D}^{(\nu)}$. The second and fourth derivatives in OS equation (2.21) can now be represented by

$$\begin{aligned}
\phi_N^{''}(y) &= (1-y^2)\, q''(y) - 4\, y\, q'(y) - 2\, q(y), \\
\phi_N^{''''}(y) &= (1-y^2)\, q''''(y) - 8\, y\, q'''(y) - 12\, q''(y)
\end{aligned}$$

where $q(y) = (1-y^2)^{-1}\phi_N(y)$ from (2.46). Using the differentiation matrix notation, they become

$$\begin{aligned}
\tilde{W}^{(2)} &= \mathbf{D}^{(2)} * \tilde{\Phi}, \\
\tilde{W}^{(4)} &= \mathbf{D}^{(4)} * \tilde{\Phi},
\end{aligned}$$

where the modified grid function is

$$\tilde{\Phi} = [\, \phi_1 \quad \phi_2 \quad \ldots \quad \phi_{N-1} \,]^T.$$

The associated differentiation matrices are defined by

$$\begin{aligned}
\mathbf{D}^{(2)} &\equiv \left(A * \tilde{D}^{(2)} - 4\, B * \tilde{D} - 2\, I \right) * C, \\
\mathbf{D}^{(4)} &\equiv \left(A * \tilde{D}^{(4)} - 8\, B * \tilde{D}^{(3)} - 12\, \tilde{D}^{(2)} \right) * C,
\end{aligned}$$

where

$$A = \begin{bmatrix} 1-y_1^2 & 0 & \ldots & 0 \\ 0 & 1-y_2^2 & \ldots & 0 \\ \vdots & \vdots & \ddots & \vdots \\ 0 & 0 & \ldots & 1-y_{N-1}^2 \end{bmatrix}, \quad B = \begin{bmatrix} y_1 & 0 & \ldots & 0 \\ 0 & y_2 & \ldots & 0 \\ \vdots & \vdots & \ddots & \vdots \\ 0 & 0 & \ldots & y_{N-1} \end{bmatrix},$$

$$C = \begin{bmatrix} (1-y_1^2)^{-1} & 0 & \dots & 0 \\ 0 & (1-y_2^2)^{-1} & \dots & 0 \\ \vdots & \vdots & \ddots & \vdots \\ 0 & 0 & \dots & (1-y_{N-1}^2)^{-1} \end{bmatrix},$$

and I is the identity matrix of size $(N-1)$.

CHAPTER 3

TWO-PHASE FLOW STABILITY

3.1 Multifluid Flow Equations

In this section, the mathematical modeling of the perturbation equations in the case of multiphase flows is discussed. Two-fluid Orr-Sommerfeld equations and the interface conditions are derived starting from the basic mathematical model of the fluid flow. The numerical implementation of the Chebyshev Pseudospectral method on the two-fluid perturbation equations is detailed.

3.1.1 Conservation Equations

Conservation laws are the fundamental physical laws that every matter and process in the universe have to comply with. Although these laws are valid in every spatial and time scale, they are generally constructed using the continuum assumption at the macro scale to model everyday applications' fluid flow.

3.1.1.1 Continuum Approach

The term "continuum" can be split into two parts in order to understand the concept clearly: "Continuous" + "medium" = "Continuum". Suppose a volume filled with material elements is shrunk to an infinitesimal size, and there are still enough elements. In that case, continuum assumption is valid, and the statistical average of the physical variables can be assigned to the entire volume [54]. Mathematical representation of

the assumption can be defined by (3.1)

$$\bar{\phi} = \lim_{\Omega \to 0} \int_{\Omega} \phi(x,t) d\Omega \tag{3.1}$$

It implies that inside such a medium, the physical variables such as mass, pressure, velocity are considered continuous. A key assumption in a continuum is that intermolecular gaps/voids are neglected [55]. Concept of continuum is depicted in Figure 3.1.

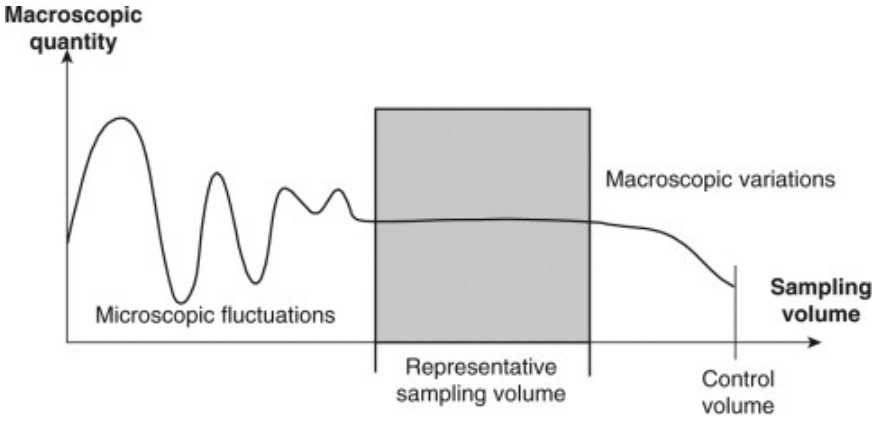

Figure 3.1: Regions where Continuum Assumption is Valid [15]

Most everyday fluids such as air and water are compatible with continuum assumption. Rarefied gases and upper atmosphere can be given as examples that continuum assumption is no longer valid. There are too few elements inside the volume regardless of the volume size. When the statistical average is taken, the average will highly differ from the individual elements and molecules inside the volume. Therefore, continuum assumption can not be made for such cases. The criterion for continuum assumption is the Knudsen number (Kn), which is defined as the ratio of the molecular mean free path length to a representative physical length scale. For continuum flow Kn < 0.01.

Continuum assumption is a method of simplification not to represent a fluid flow problem by molecular dynamics. Molecular dynamics represent micro-scale analysis and solution for a physical case. However, most everyday problems are macro-scale problems. These problems can take near infinite time to analyze and solve by micro-scale level approaches. Therefore, continuum assumption is made in order to project the physics of micro-scale to macro-scale level.

Definition of phasic interfaces, boundaries, shocks as discontinuities are results of continuum assumption. The difference between molecular and continuum level perspective to the multiphase interface can be observed in Figure 3.2.

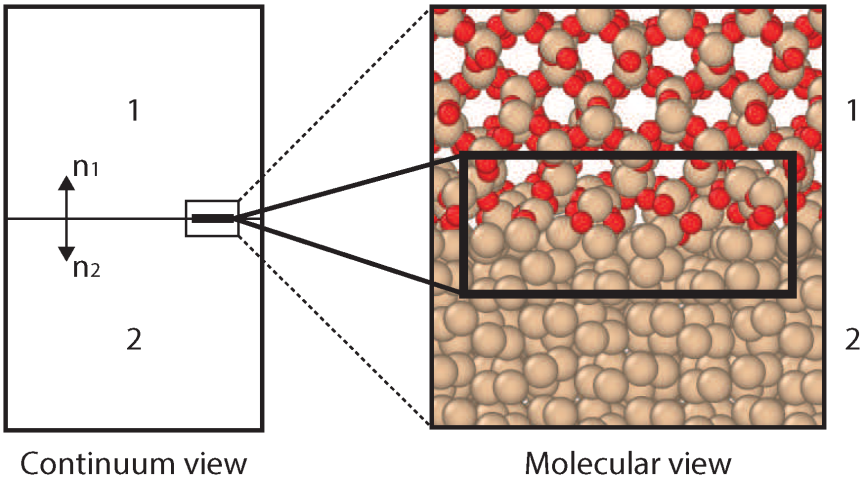

Figure 3.2: Molecular vs Continuum perspective of Phasic Interface [16]

With continuum assumption, system level analysis (macro-level) can be done with physical conservation laws.

3.1.1.2 Reynolds Transport Theorem

Reynolds Transport Theorem is a tool to construct conservation system equations using control volume (material body) analysis [56, 57].

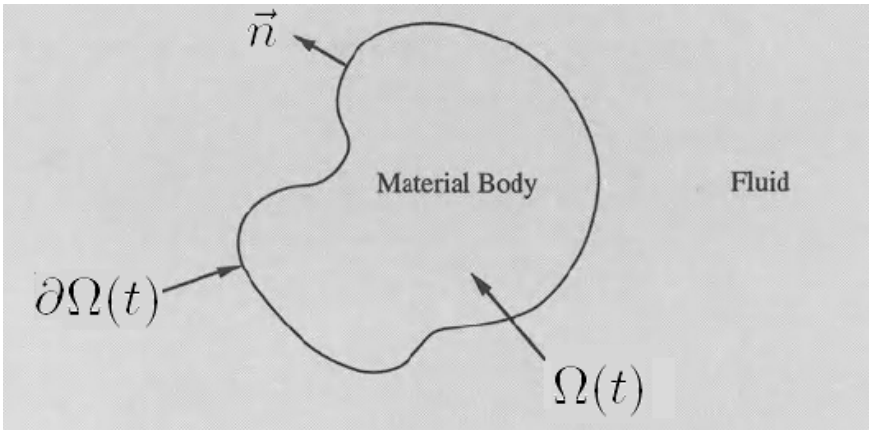

Figure 3.3: Single fluid arbitrary control volume [17]

Let $\Omega(t)$ be a region in Euclidean space with boundary $\partial\Omega(t)$ and the outward unit normal $\vec{n}(\vec{x},t)$ to the boundary (Figure 3.3). Let $\vec{x}=\vec{x}(t)$ be the positions of points and $\vec{V}(\vec{x},t)$ be the velocity field in the region containing the quantity $q(\vec{x},t)$ that is Q per volume Ω. Then

$$\begin{aligned}\frac{dQ}{dt} &= \frac{d}{dt}\int_{\Omega(t)} q(\vec{x},t)\,d\Omega = \frac{d}{dt}\int_{\Omega_0} q(\vec{x},t)\,J d\Omega_0 \\ &= \int_{\Omega_0}\left(\frac{dq}{dt}J + q\frac{dJ}{dt}\right)\,d\Omega_0 = \int_{\Omega_0}\left(\frac{dq}{dt} + q\left(\nabla\cdot\vec{V}\right)\right)\,J d\Omega_0 \\ &= \int_{\Omega(t)}\left(\frac{dq}{dt} + q\left(\nabla\cdot\vec{V}\right)\right)\,d\Omega = \int_{\Omega(t)}\left(\frac{\partial q}{\partial t} + \nabla\cdot\left(q\vec{V}\right)\right)\,d\Omega\end{aligned}$$

where Ω_0 is a reference configuration of the region $\Omega(t)$ and J is the Jacobian of transformation from Ω_0 to $\Omega(t)$ such that $dJ/dt = J\left(\nabla\cdot\vec{V}\right)$. Using the divergence theorem, it yields the Reynolds Transport equation

$$\frac{dQ}{dt} = \int_{\Omega}\frac{\partial q}{\partial t}\,d\Omega + \int_{\partial\Omega} q\,\vec{V}\cdot\vec{n}\,dS. \tag{3.2}$$

This mathematical process leading to (3.2) is a generalization of the Leibniz rule and, it can be applied to any conserved quantity q.

Mass Conservation

The quantity of mass inside a system will remain constant independent of the processes inside or outside of the system, that is:

$$\frac{d\,(m)}{dt} = 0.$$

For a control (material) volume Ω, it becomes:

$$\int_{\Omega}\left(\frac{\partial\rho}{\partial t} + \nabla\cdot(\rho\vec{u})\right)\,d\Omega = \int_{\Omega}\frac{\partial\rho}{\partial t}\,d\Omega + \int_{\partial\Omega}\rho\vec{u}\cdot\vec{n}\,dS = 0, \tag{3.3}$$

where ρ is the density of the fluid.

Momentum Conservation

The quantity of momentum inside a system will remain constant independent of the processes inside or outside of the system, that is:

$$\frac{d\,(m\vec{u})}{dt} = \sum\vec{F}$$

where $\vec{F}$ stands for the surface and body forces. For a control (material) volume Ω, it becomes::

$$\int_{\Omega} \frac{\partial (\rho \vec{u})}{\partial t} d\Omega + \int_{\partial\Omega} \rho \vec{u} (\vec{u} \cdot \vec{n}) \, dS = \int_{\Omega} \left(\nabla \cdot \vec{\vec{\sigma}} + \rho \vec{f_b} \right) d\Omega \tag{3.4}$$

where $\vec{f_b}$ represents body force and $\vec{\vec{\sigma}}$ the stress tensor.

Energy Conservation

The internal energy e of a system will remain constant independent of the processes inside or outside of the system, that is

$$\frac{d (m\, e)}{dt} = \sum W - \sum Q.$$

For a control (material) volume Ω, it can be represented by:

$$\int_{\Omega} \frac{\partial (\rho\, e)}{\partial t} \, d\Omega + \int_{\partial\Omega} \rho\, e\, \vec{u} \cdot \vec{n} \, dS = \sum W - \sum Q \tag{3.5}$$

where W and Q represent work done on/by the system and heat transfer from/to the system, respectively.

3.1.2 Jump Conditions

Conservation laws are expressed as partial differential equations (PDEs). However, PDEs require continuous fields in order to be valid models [24]. Some physical phenomenons such as shocks, contact discontinuities, and material interfaces are considered to be mathematical discontinuities due to their very small thickness when it is compared with the characteristic length of macroscopic processes [45]. Across these interfaces, the fluids or substances are divided geometrically, and due to this division, each side of the interface represents different material properties [58], thus different thermodynamic and flow properties. These discontinuities violate the continuous field condition that is necessary for the validity of the governing PDEs. However, discontinuous or not, conservation laws are still valid.

In order to overcome these issues, conservation laws are applied to discontinuities that separate regions occupied by the body where the fields are smooth and that the flow variables have definite but different limiting values on either side in the form of

a jump. The associated jump conditions for the flow variables are then derived for handling discontinuities within the context of conservation laws [59].

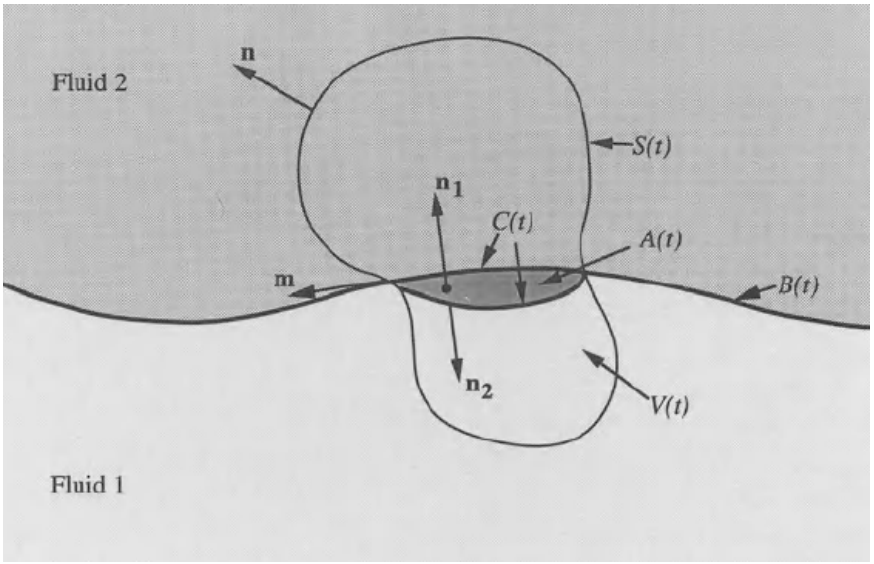

Figure 3.4: Representation of interface as discontinuity inside a control volume [17]

This is done by placing an arbitrary control volume which captures a part of the interface inside the multi-fluid problem as in Figure 3.4, yielding the jump conditions for mass, momentum, and energy across the interface as follows:

Mass jump condition

$$\left[\!\left[\rho \left(\vec{u} - \vec{u}_i \right) \right]\!\right] \cdot \vec{n} = 0 \tag{3.6}$$

Momentum jump condition

$$\left[\!\left[\rho \vec{u} \left(\vec{u} - \vec{u}_i \right) + \vec{\vec{\sigma}} \right]\!\right] \cdot \vec{n} = \vec{F}_i \tag{3.7}$$

Energy jump condition

$$\left[\!\left[\rho \left(e + \tfrac{1}{2} \vec{u}^2 \left(\vec{u} - \vec{u}_i \right) \right) + \left(\vec{\vec{\sigma}} \cdot \vec{u} - \vec{q} \right) \right]\!\right] \cdot \vec{n} = e_i \tag{3.8}$$

where subscript i denotes the interface, $\vec{F}_i$ and e_i are the momentum and energy exchange at the interface, respectively, $\vec{\vec{\sigma}}$ the stress tensor and $\vec{q}$ the heat flux vector. Here $\left[\!\left[\phi \right]\!\right] = \phi_2 - \phi_1$ denotes the jump operator applied on a flow variable ϕ across the interface separating Fluid 1 and 2.

3.2 Two-Fluid Flow Stability Equations Derivation

3.2.1 Orr-Sommerfeld Equations for Two-Fluid flows

We consider two fluids that are flowing parallel to each other with different mean flow velocity profiles, and they are separated by an interface as shown in Figure 3.5.

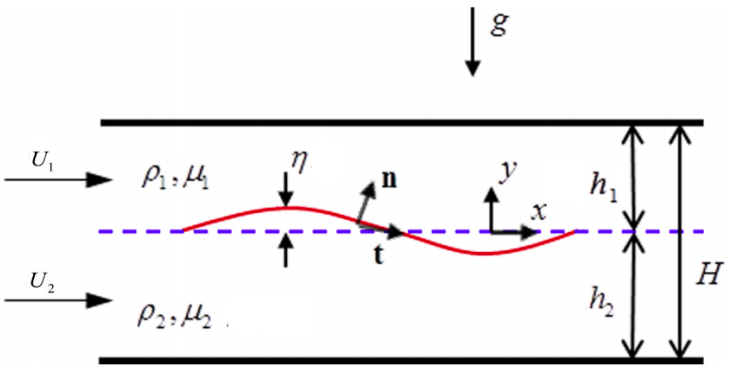

Figure 3.5: Two-phase parallel flow [18]

Squire's theorem is also valid for two-phase flows. Thus, 2D disturbances, regardless of their physical origins, are still the most critical disturbances for the investigation of instability in this case [60, 61, 62].

3.2.1.1 Orr-Sommerfeld Equations

The Orr-Sommerfeld equation that was derived for a single fluid can be extended to the two-fluid case by considering the different material properties of fluids at different sides of the interface in the form of ratios with respect to the non-dimensional form of the equations. Orr-Sommerfeld equations for fluids 1 and 2 at different sides of the interface then have the form [42, 36, 30]

$$\phi_1'''' - 2\alpha^2\phi_1 + \alpha^4\phi_1 = i\,\alpha Re\left((U_1 - c)\left(\phi_1'' - \alpha^2\phi_1\right) - \phi\,U_1''\right), \tag{3.9a}$$

$$\phi_2'''' - 2\alpha^2\phi_2'' + \alpha^4\phi_2 = i\,\alpha\frac{Re\,r}{m}\left((U_2 - c)\left(\phi_2'' - \alpha^2\phi_2\right) - \phi\,U_2''\right) \tag{3.9b}$$

where ϕ_1 and ϕ_2 are the amplitudes of the corresponding streamfunctions in the normal mode representations as in (2.20).

As stated in (2.22), Reynolds number (Re) and α were the only parameters which are involved in characterizing the perturbations for one-fluid flow. However, as it can be seen from Figure 3.5 and (3.9) for two-fluid flows, six non-dimensionless numbers are needed to characterize the perturbation equations. These non-dimensional numbers are [42, 36]:

$$Re = \frac{\rho_1 U_\tau d_1}{\mu_1} \quad : \text{Reynolds number} \tag{3.10a}$$

$$m = \frac{\mu_2}{\mu_1} \quad : \text{Ratio of viscosities} \tag{3.10b}$$

$$r = \frac{\rho_2}{\rho_1} \quad : \text{Ratio of densities} \tag{3.10c}$$

$$n = \frac{h_2}{h_1} = \frac{d_2}{d_1} \quad : \text{Ratio of heights} \tag{3.10d}$$

$$Fr = \frac{\rho_1 U_\tau^2}{g\left(\rho_1 - \rho_2\right) d_1} \quad : \text{Froude number} \tag{3.10e}$$

$$We = \frac{\rho_1 U_\tau^2 d_1}{\sigma} \quad : \text{Weber number} \tag{3.10f}$$

where $\tau = \mu_1 \, \partial u / \partial y$ denotes shear stress at the interface and $U_\tau = \tau \, d_1 / \mu_1$ is the characteristic velocity at interface. Alternatively, the velocity of the mean flow at the interface U_0 may also be used as characteristic velocity. Symbols of d_i and h_i can be considered as interchangeable which both of them represent the height of the current phase (i) in y direction.

3.2.1.2 Boundary Conditions

At the wall or at the boundaries at infinity (if any), perturbations of the flow quantities are set equal to zero, namely,

No-slip boundary condition (vanishing tangential velocity):

$$u(y_U) = u(y_L) = 0 \implies \phi(y_U) = \phi(y_L) = 0 \tag{3.11}$$

No-penetration boundary condition (vanishing normal velocity) :

$$v(y_U) = v(y_L) = 0 \implies \phi^{'}(y_U) = \phi^{'}(y_L) = 0 \tag{3.12}$$

where subscripts (U) and (L) refer to Upper and Lower boundaries, respectively. Here, the velocity boundary conditions are also expressed in terms of the amplitude of the streamfunction.

In a two-fluid problem, there are two Orr-Sommerfeld equations. This creates the necessity of four additional conditions, after two boundary conditions for each fluid is applied at the walls (or infinity), in order to obtain a well-posed problem. This is supplied by the jump conditions at the interface between the two-fluids that will be referred to as interface conditions.

3.2.2 Interface Conditions

Jump conditions which are given by (3.6), (3.7) and (3.8) are used to derive kinematic and dynamic interface conditions at the interface. Detailed derivations of the interface conditions from conservation equations can be found in [17, 63, 58].

3.2.2.1 Kinematic Boundary Conditions

The jump condition for mass conservation (3.6) when applied to both sides of the interface yields [17],

$$\rho_1(\vec{u}_1 - \vec{u}_i) \cdot \vec{n}_i - \rho_2(\vec{u}_2 - \vec{u}_i) \cdot \vec{n}_i = 0. \tag{3.13}$$

The only way to satisfy (3.13) is $\vec{u}_1 = \vec{u}_2$ which, in 2D, yields the continuity condition of the tangential velocity components

$$u_1 = u_2 \tag{3.14}$$

at the interface. Note that if the fluids are inviscid, this condition is not valid anymore. And the continuity conditions of the normal velocity components

$$v_1 = v_2 \tag{3.15}$$

at the interface. This condition is valid regardless of fluids being inviscid or viscous.

The equations (3.14) and (3.15) will be referred to as **Interface Conditions 1 and 2**, respectively. These conditions are applied at the interface and the normal mode perturbation analysis of the interface needs to be considered in order to construct the associated interface conditions for the Orr-Sommerfeld Equations.

Deviation Derivation

We consider the interface as a free surface measured from the bottom boundary by the y coordinate as shown in the Figure 3.6.

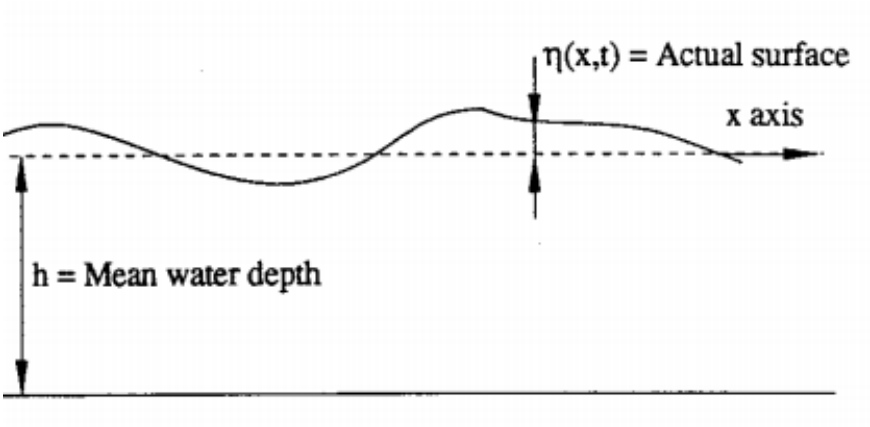

Figure 3.6: Deviation of interface with respect to the y coordinate [19]

In accordance with the normal mode analysis adopted in the derivation of the Orr-Sommerfeld equation, the deviation of the interface in y is modeled as a normal mode:

$$y = \eta(x,t) = Ne^{i\alpha(x-ct)} \tag{3.16}$$

In order to construct a mathematical description, the displacement of a fluid particle from point 1 $(\eta(x_1,t_1))$ to point 2 $(\eta(x_2,t_2))$ is shown graphically in Figure 3.7.

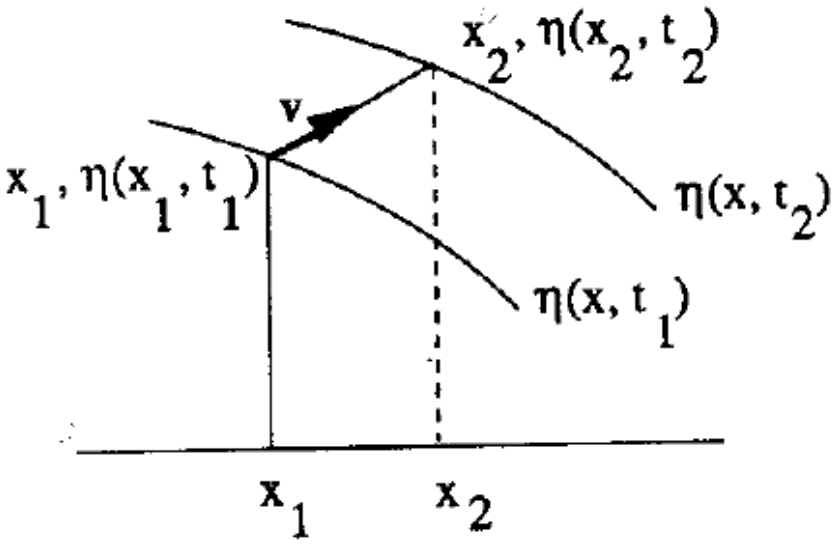

Figure 3.7: Displacement of a point on the interface [19]

It translates into the mathematical language as follows:

$$\eta(x_2, t_2) = \eta(x_1, t_1) + v(t_2 - t_1) \quad \text{and} \quad x_2 = x_1 + u(t_2 - t_1).$$

Using the linear approximation:

$$\eta(x_2, t_2) = \eta(x_1, t_2) + \frac{\partial \eta}{\partial x}(x_2 - x_1),$$

the displacement of the interface becomes

$$\eta(x_1, t_2) - \eta(x_1, t_1) + \frac{\partial \eta}{\partial x}(x_2 - x_1) = v(t_2 - t_1),$$

and thus

$$\frac{\eta(x_1, t_2) - \eta(x_1, t_1)}{(t_2 - t_1)} + \frac{\partial \eta}{\partial x}\frac{(x_2 - x_1)}{(t_2 - t_1)} = v.$$

For infinitesimal deviations, it leads to the kinematic condition at $y = \eta$:

$$\frac{d\eta}{dt} = \frac{\partial \eta}{\partial t} + \frac{\partial \eta}{\partial x}u = v. \tag{3.17}$$

Physical interpretation of (3.17) is that a fluid particle at a free surface can never leave the surface at all times. It is kind of free surface boundary condition version of conservation of mass [19]. Since forces and thermodynamic variables are not involved in this derivation, it is therefore called kinematic condition.

In order to obtain an expression for the amplitude N of η in normal mode representation (3.16) and the perturbation of the flow field (2.12a) is introduced into (3.17) to get the expression at interface location ($y = \eta$):

$$\left(\frac{\partial \eta}{\partial t} + (U+u)\frac{\partial \eta}{\partial x}\right) = v = -i\alpha\phi(\eta)e^{i\alpha(x-ct)}$$

which after linearization it becomes

$$\eta = \left(\frac{\phi(0)}{c-U(0)}\right)e^{i\alpha(x-ct)}$$

and so N turns out to be a constant [27]

$$N = \frac{\phi(0)}{c-U(0)}. \tag{3.18}$$

Here, the linear approximation

$$q\big|_{y=\eta} \approx q\big|_{y=0} + q'\big|_{y=0}\,\eta$$

is used for q representing a generic quantity and products of perturbed quantities are omitted.

Derivation of the interface conditions in form of normal modes can then be obtained as follows:

Interface Condition 1 (Continuity of tangential velocity at $y = \eta$)

$$\phi_1(0) = \phi_2(0) \tag{3.19}$$

that is obtained from (3.14).

Interface Condition 2 (Continuity of normal velocity at $y = \eta$)

Using the continuity equation:

$$\frac{\partial u}{\partial x} + \frac{\partial v}{\partial y} = 0 \implies \frac{\partial u}{\partial x} = -\frac{\partial v}{\partial y}$$

and (3.17), one gets:

$$\begin{aligned}
\frac{\partial u}{\partial x} &= -\frac{\partial}{\partial y}\left(\frac{\partial \eta}{\partial t} + U\frac{\partial \eta}{\partial x}\right), \\
\phi^{'}(i\alpha) &= -\frac{\partial}{\partial y}\left(N(-i\alpha c) + Ui\alpha N\right), \\
\phi^{'}(i\alpha) &= -U^{'}i\alpha N, \\
\phi^{'} &= -U^{'}N,
\end{aligned}$$

and thus

$$\phi^{'}(0) + U^{'}(0)\left(\frac{\phi(0)}{c - U(0)}\right) = 0.$$

The condition (3.15) becomes:

$$\phi_1^{'}(0) + U_1^{'}(0)\left(\frac{\phi_1(0)}{c - U_1(0)}\right) = \phi_2^{'}(0) + U_2^{'}(0)\left(\frac{\phi_2(0)}{c - U_2(0)}\right). \tag{3.20}$$

3.2.2.2 Dynamic Boundary Conditions

They actually result form the implementation of conservation of momentum at interfaces. The stress balance at the interface requires normal and tangential components of the stress to be equal there [17].

In 2D, the Momentum Jump Condition (3.7) at the interface ($y = \eta$) becomes:

$$\left(\rho_1 \vec{u_1}\vec{u_1} - \rho_1 \vec{u_1}\vec{u_i} - \rho_2 \vec{u_2}\vec{u_2} - \rho_2 \vec{u_2}\vec{u_i} + \vec{\vec{\sigma}}_1 - \vec{\vec{\sigma}}_2\right) \cdot \vec{n} = \vec{F_i} \tag{3.21}$$

When the Kinematic Boundary Conditions 3.14 and 3.15 are substituted into (3.21), it results in the Dynamic Boundary Condition in the absence of momentum exchange at the interface:

$$\vec{\vec{\sigma}}_1 = \vec{\vec{\sigma}}_2 \tag{3.22}$$

where the stress tensor is given by [63, 64]

$$\vec{\vec{\sigma}} = -p\vec{\vec{I}} + \vec{\vec{\tau}}. \tag{3.23}$$

Pressure (p) by definition always acts normal to interface. The viscous stress tensor ($\vec{\vec{\tau}}$) term have both normal and tangential components. The viscous stress tensor can not be calculated directly and they have to be modelled. Their relation with strain rates are established linearly for Newtonian fluids and they for incompressible fluids are as follows:

$$\tau_{xx} = 2\mu\left(\frac{\partial u}{\partial x}\right), \quad \tau_{xy} = \tau_{yx} = \mu\left(\frac{\partial u}{\partial y} + \frac{\partial v}{\partial x}\right), \quad \tau_{yy} = 2\mu\left(\frac{\partial v}{\partial y}\right). \tag{3.24}$$

Besides the gravity effect, one of the causes of the momentum exchange at the interface (3.7) is the surface tension.

$$\vec{F_i} = \frac{\sigma}{R_m}\vec{n} + \rho g h\, \vec{e}_y \tag{3.25}$$

where the normal vector $\vec{n}$ on the inter-surface $S(x, y, t) = y - \eta(x, t) = 0$ is defined by

$$\vec{n} = \nabla S / \|\nabla S\|.$$

Body forces like gravity and magnetic field can also affect the momentum field inside the domain. Contrary to surface forces, the direction of body forces is only dependent on the global coordinates.

Dynamic Boundary Conditions in the normal $\vec{n}$ and tangential $\vec{t}$ directions with respect to the interface ($y = \eta$) are given as follows [17]:

Normal Direction:

$$-(p_1 - p_2) + \vec{n} \cdot \left(\vec{\vec{\tau}}_1 - \vec{\vec{\tau}}_2\right) \cdot \vec{n} = \frac{\sigma}{R_m} + (\rho_2 - \rho_1) g\eta. \tag{3.26}$$

Tangential Direction:

$$\vec{n}_i \cdot \left(\vec{\vec{\tau}}_1 - \vec{\vec{\tau}}_2\right) \cdot \vec{t} = 0. \tag{3.27}$$

Interface Condition 3 (Balance of tangential stresses at $y = \eta$) [27, 34]:

Dynamic Boundary Conditions in the tangential $\vec{t}$ direction (3.27) after the substitution of the perturbation flow field (2.12a) and linearization about $y = 0$ reads:

$$\mu_1 \left(\left(\frac{\partial u_1}{\partial y} + \frac{\partial v_1}{\partial x} \right) + \eta U_1'' \right) \Bigg|_{y=0} = \mu_2 \left(\left(\frac{\partial u_2}{\partial y} + \frac{\partial v_2}{\partial x} \right) + \eta U_2'' \right) \Bigg|_{y=0}. \tag{3.28}$$

In the form of the normal modes, it becomes

$$\phi_1''(0) + \alpha^2 \phi_1(0) + U_1''(0) \left(\frac{\phi_1(0)}{c - U_1(0)} \right) = m \left(\phi_2''(0) + \alpha^2 \phi_2(0) + U_2''(0) \left(\frac{\phi_2(0)}{c - U_2(0)} \right) \right). \tag{3.29}$$

Interface Condition 4 (Balance of normal stresses $y = \eta$) [27, 25, 28]:

The Momentum Jump Condition (3.7) in the normal direction reads:

$$\left[\!\left[-p + 2\mu \left(\frac{\partial v}{\partial y} \right) \right]\!\right] = \sigma \frac{\partial^2 \eta}{\partial x^2} + (\rho_2 - \rho_1) g\eta$$

where $\partial^2\eta/\partial x^2 = R_m^{-1}$ is the curvature. Scaling velocity by U_0, the time by h_1/U_0 and the pressure by $\rho_1 U_0^2$ yields the non-dimensional form:

$$\left[\!\left[-p + \frac{2}{Re}\left(\frac{\partial v}{\partial y}\right)\right]\!\right] = \frac{1}{We}\frac{\partial^2\eta}{\partial x^2} - \frac{1}{Fr}\eta$$

where

$$Fr = \frac{\rho_1 U_0^2}{g\left(\rho_1 - \rho_2\right)h_1} \quad : \quad \text{Froude number,}$$

$$We = \frac{\rho_1 U_0^2 h_1}{\sigma} \quad : \quad \text{Weber number,}$$

$$Re = \frac{\rho_1 U_0 h_1}{\mu} \quad : \quad \text{Reynolds number.}$$

In terms of the normal modes:

$$\left[\!\left[f + \frac{2}{Re} i\alpha\phi^{'}\right]\!\right] = \frac{1}{We}\alpha^2 N + \frac{1}{Fr}N \tag{3.30}$$

where f is the amplitude of pressure in normal mode representation $p = f\, e^{i\alpha(x-ct)}$. An expression for f can be derived by using (2.16a) and (2.16b) in the streamfunction and normal modes formulations to get

$$f = -(U-c)\phi^{'} + U\phi + \frac{1}{i\alpha Re}(\phi^{'''} - \alpha^2\phi^{'}). \tag{3.31}$$

When (3.31) is substituted into (3.30), it yields

$$\left[\!\left[i\alpha Re\left((c-U)\,\phi^{'} + U\phi\right) + \phi^{'''} - 3\alpha^2\phi^{'}\right]\!\right] = i\alpha ReN\left(\frac{1}{Fr} + \frac{\alpha^2}{We}\right). \tag{3.32}$$

After expanding (3.32) across the interface separating Fluid 1 and 2, it becomes:

$$\begin{aligned} i\alpha Re\left[(c-U(0))\,\phi_1^{'}(0) + U(0)\phi_1(0)\right] + \left(\phi_1^{'''}(0) - 3\alpha^2\phi_1^{'}(0)\right) \\ - i\alpha rRe\left[(c-U(0))\,\phi_2^{'}(0) + U(0)\phi_2(0)\right] - m\left(\phi_2^{'''}(0) - 3\alpha^2\phi_2^{'}(0)\right) \\ = i\alpha Re\left(\frac{\phi_1(0)}{c-U(0)}\right)\left[\frac{1}{Fr} + \frac{\alpha^2}{We}\right]. \end{aligned} \tag{3.33}$$

Equation (3.33) combines the effects of gravity, surface tension, pressure, and normal component of the viscous stresses.

Similarity between Boundary and Interface Conditions

This is a short discussion about the "difference" or the "similarity" of boundary and interface conditions. "Boundary condition" is generally a mathematical term. It represents the values of the fields at the "boundaries" of the domain. However, in fluid mechanics, these boundaries have physical meaning. They are either a wall or shoots to infinity or another substance. For the wall boundary condition, every boundary condition is actually an interface condition where the other side of the wall is made of another substance.

Walls are actually stationary of moving phasic interfaces where conservation equations must be valid. For example, at stationary walls velocity of the fluid has to be equal to zero for viscous fluids. This is due to the walls being stationary. If the walls are moving, the velocity of the fluid will be equal to wall velocity at the wall. In fact, this example is an instance of a jump condition for mass conservation. Similar derivations can be done for momentum and energy.

Therefore, it can be said that bounded boundary conditions for fluid mechanics are actually interface conditions.

3.2.2.3 "Energy or Temperature" Condition

Due to interface conditions for the conservation of energy equation, temperatures (T) at the interface must be equal.

$$T_1 = T_2 \tag{3.34}$$

Unlike the other interface conditions, the condition (3.34) can only be realized if there is a heat diffusion process across the interface. For example, for Euler equations, even if the flow is compressible, (3.34) will not be realized due to the absence of the heat diffusion process.

The case is similar to incompressible flow. The energy equation is already decoupled from the equations system. Therefore, the condition which is presented in (3.34) is not implemented in this work.

3.2.3 Wellposedness of Problem

Two-fluid Orr-Sommerfeld Equations, (3.9a) and (3.9b) are of 4th order ODEs, each. Thus, they require to be supplemented by 8 external (closure) conditions such as boundary conditions and interface conditions.

There are 4 Boundary Conditions, (3.11 - 3.12) that involve the amplitude dependent variable ϕ and its derivatives, 2 at the bottom and 2 at the top surfaces. Interface Conditions, (3.19, 3.20, 3.29 and 3.33) are 4 more conditions from Kinematic and Dynamic Conditions across the interface. These 8 conditions render the system of equations well-posed and solvable.

System of Equations [42]

Governing Equations:

$$\phi_1^{''''} - 2\alpha^2\phi_1 + \alpha^4\phi_1 = i\,\alpha Re\left((U_1 - c)\left(\phi_1{}'' - \alpha^2\phi_1\right) - \phi\, U_1^{''}\right), \tag{3.35a}$$

$$\phi_2^{''''} - 2\alpha^2\phi_2^{''} + \alpha^4\phi_2 = i\,\alpha\frac{Re\,r}{m}\left((U_2 - c)\left(\phi_2{}'' - \alpha^2\phi_2\right) - \phi\, U_2^{''}\right) \tag{3.35b}$$

Boundary Conditions at Upper Boundary (U) of Fluid 1 and Lower Boundary (L) of Fluid 2:

$$\phi_1(y_U) = \phi_2(y_L) = \phi_1^{'}(y_U) = \phi_2^{'}(y_L) = 0 \tag{3.36}$$

Interface Conditions at $y = \eta \approx 0$:

$$\phi_1(0) = \phi_2(0), \tag{3.37}$$

$$\phi_1^{'}(0) + U_1^{'}(0)\left(\frac{\phi_1(0)}{c - U_1(0)}\right) = \phi_2^{'}(0) + U_2^{'}(0)\left(\frac{\phi_2(0)}{c - U_2(0)}\right), \tag{3.38}$$

$$\phi_1^{''}(0) + \alpha^2\phi_1(0) + U_1^{''}(0)\left(\frac{\phi_1(0)}{c - U_1(0)}\right) = m\left(\phi_2^{''}(0) + \alpha^2\phi_2(0) + U_2^{''}(0)\left(\frac{\phi_2(0)}{c - U_2(0)}\right)\right), \tag{3.39}$$

$$i\alpha Re\left[(c-U_1(0))\,\phi_1'(0)+U_1(0)\phi_1(0)\right]+\left(\phi_1'''(0)-3\alpha^2\phi_1'(0)\right)$$
$$-i\alpha rRe\left[(c-U_2(0))\,\phi_2'(0)+U_2(0)\phi_2(0)\right]-m\left(\phi_2'''(0)-3\alpha^2\phi_2'(0)\right)$$
$$=i\alpha Re\left(\frac{\phi_1(0)}{c-U_1(0)}\right)\left[\frac{1}{Fr}+\frac{\alpha^2}{We}\right]. \quad (3.40)$$

This system of equations, (3.35 - 3.40), form a well-posed generalized differential eigenvalue problem for the temporal eigenvalue c satisfying the dispersion relation

$$c=c(R,m,r,F,S,\alpha). \quad (3.41)$$

The numerical methods for solving this equation system will be discussed in the following sections.

3.3 Two-Phase Eigenvalue Problem

3.3.1 Mathematical Properties of Orr-Sommerfeld Equations

The Original equations, 2D incompressible Navier-Stokes equations, (2.8) and (2.9), are 2^{nd} order PDEs with 3 unknowns of u, v, and p. These unknowns are dependent on spatial coordinates x and y, and time t.

In order to eliminate of the pressure gradient term from the linearized perturbation equations (2.16), they are cross differentiated in space and combined. This operation results in a 3^{rd} order equation (2.17) governing u and v. Introducing the streamfunction formulation (2.18) decreases the number of unknowns to the streamfunction φ, but increases the order of the equation (2.19) to 4. Introducing the normal modes representation (2.20) next, results in the 4^{th} Orr-Sommerfeld equation (2.21) and reduces the number of independent variables to y, only.

3.3.2 Algebraic Point of View

As it is mentioned before, (3.35 - 3.40) form a differential eigenvalue problem. After discretization by Chebyshev Pseudospectral Method (CPM) based on the Chebyshev

polynomial representation (2.44), it reduces to an algebraic generalized eigenvalue problem in the form:

$$\big[A\big]\,\Phi = c\,\big[B\big]\,\Phi \tag{3.42}$$

where $[A]$ and $[B]$ represent Multiphase System Matrices (MM). The vector Φ in (3.42) is the combined grid function representation of discretized streamfunction amplitude variables $\phi_1(y)$ and $\phi_2(y)$ in the form

$$\Phi = \big[\,(\phi_1)_0 \quad (\phi_1)_1 \quad \ldots \quad (\phi_1)_N \quad (\phi_2)_0 \quad (\phi_2)_1 \quad \ldots \quad (\phi_2)_M\,\big]^T \tag{3.43}$$

where the indexing should be read as follows:

$$\begin{aligned}(\phi_1)_0 &\approx \phi_1(y_L)\\ (\phi_1)_N &\approx \phi_1(0)\\ (\phi_2)_0 &\approx \phi_2(0)\\ (\phi_2)_M &\approx \phi_2(y_U).\end{aligned}$$

3.3.2.1 OS Equations for Each Phase

In the case of the temporal instability problem, Orr-Sommerfeld equations are linear in the eigenvalue c. Therefore, after discretization, linear algebraic generalized eigenvalue problem (3.42) results. The constituents of the MM matrices that correspond to discretized form of the Orr-Sommerfeld equations for each fluid are as follows:

$$\phi_1'''' - 2\alpha^2\phi_1'' + \alpha^4\phi_1 + i\alpha Re\phi_1 U_1'' - i\alpha Re U_1\left(\phi_1'' - \alpha^2\phi_1\right) \overset{CPM}{\Longrightarrow}$$

$$\big[\,A_1\,\big] \equiv D_N^4 - 2\alpha^2 D_N^2 + \alpha^4 I_N + i\alpha Re\left((D_N^2 U_1)\right)$$

$$- i\alpha Re\left((U_1)\right)\left(D_N^2 - \alpha^2 I_N\right) \tag{3.45}$$

$$-i\alpha Re\left(\phi_1'' - \alpha^2\phi_1\right) \overset{CPM}{\Longrightarrow} \big[\,B_1\,\big] \equiv -i\alpha Re\left(D_N^2 - \alpha^2 I_N\right) \tag{3.46}$$

$$\phi_2'''' - 2\alpha^2\phi_2'' + \alpha^4\phi_2 + i\alpha\, Re\,(r/m)\,\phi_2 U_2'' - i\alpha\, Re\,(r/m)\,U_1\left(\phi_2'' - \alpha^2\phi_2\right) \overset{CPM}{\Longrightarrow}$$

$$\big[\,A_2\,\big] \equiv D_M^4 - 2\alpha^2 D_M^2 + \alpha^4 I_M + i\alpha\, Re\,(r/m)\left((D_M^2 U_2)\right)$$

$$- i\alpha\, Re\,(r/m)\left((U_1)\right)\left(D_M^2 - \alpha^2 I_M\right) \tag{3.47}$$

$$-i\alpha\, Re\,(r/m)\left(\phi_2'' - \alpha^2\phi_2\right) \overset{CPM}{\Longrightarrow} \left[\, B_2 \,\right] \equiv -i\alpha\, Re(r/m)\, \left(D_M^2 - \alpha^2 I_M\right) \tag{3.48}$$

where D_N denotes the Chebyshev differentiation matrix as defined in (2.41) corresponding to the modal expansion (2.35) of order N. The notation $((\cdot))$ is used to denote the diagonalization operation as in (*diag*) of Matlab. Chebyshev polynomials are defined in the standard interval $[-1, 1]$, so two linear maps are used here to map the standard interval to $[y_L, 0]$ and $[0, y_U]$. This requires an appropriate scaling to be used on the corresponding differentiation matrices as well.

Using these matrix operators, MM matrices in (3.42) can be constructed as follows:

$$\left[\, A \,\right] = \begin{bmatrix} A_1 & O_{NM} \\ O_{MN} & A_2 \end{bmatrix} \quad \text{and} \quad \left[\, B \,\right] = \begin{bmatrix} B_1 & O_{NM} \\ O_{MN} & B_2 \end{bmatrix} \tag{3.49}$$

where O_{NM} is the zero matrix of order $(N+1) \times (M+1)$.

3.3.2.2 Boundary Conditions

Boundary conditions (3.36) for the system of equations (3.42) do not have the eigenvalue parameter c. Therefore, they will only appear in the coefficient matrix A. These conditions are placed in the first and the last two rows of the matrix A in the form of external equations as mentioned in Section (2.2.4), while corresponding rows in the matrix B are zeroed as follows:

$$\left[\, A_1 \,\right] = \begin{bmatrix} 1 & 0 & \dots & 0 \\ (D_N)_{00} & (D_N)_{01} & \dots & (D_N)_{0N} \\ & \tilde{A}_1 & & \end{bmatrix},$$

$$\left[\, A_2 \,\right] = \begin{bmatrix} & \tilde{A}_2 & & \\ (D_M)_{M0} & (D_M)_{M1} & \dots & (D_M)_{MM} \\ 0 & 0 & \dots & 1 \end{bmatrix},$$

$$\left[\, B_1 \,\right] = \begin{bmatrix} 0 & 0 & \dots & 0 \\ 0 & 0 & \dots & 0 \\ & \tilde{B}_1 & & \end{bmatrix} \quad \text{and} \quad \left[\, B_2 \,\right] = \begin{bmatrix} & \tilde{B}_2 & & \\ 0 & 0 & \dots & 0 \\ 0 & 0 & \dots & 0 \end{bmatrix}.$$

3.3.2.3 Interface Conditions

As it is done in the case of boundary conditions, the interface conditions (3.37-3.40) will be incorporated into MM matrices by replacing certain rows by the discretized from of the interface conditions. There are 4 interface conditions and so the last two rows of $\left[\, A_1, B_1 \,\right]$ and the first two rows of $\left[\, A_2, B_2 \,\right]$ will be replaced by the interface conditions.

Interface Condition 1 (3.37), tangential velocity balance

$$\phi_1(0) = \phi_2(0) \equiv \phi(0)$$

does not contain the eigenvalue parameter c. Therefore, this interface condition will only reside in the coefficient matrix A, and the corresponding rows in the matrix B will be zeroed.

Interface Condition 2 (3.38), normal velocity balance, contains the eigenvalue parameter c. By using (3.37) and the fact that the primary flow is continuous across the interface

$$U_1(0) = U_2(0) \equiv U(0)$$

it can be simplified to read:

$$\phi(0)\left(U_1^{'}(0) - U_2^{'}(0)\right) = \tilde{c}\left(\phi_2^{'}(0) - \phi_1^{'}(0)\right) \tag{3.50}$$

where

$$\tilde{c} = c - U(0)$$

that is the problem in a frame that moves at the interfacial speed $U(0)$. It will reside both in the coefficient matrix A and B as follows:

$$\begin{aligned} \phi(0)\left(U_1^{'}(0) - U_2^{'}(0)\right) &\longrightarrow A \\ \left(\phi_2^{'}(0) - \phi_1^{'}(0)\right) &\longrightarrow B. \end{aligned}$$

Interface Condition 3 (3.39), tangential stress balance, contains the eigenvalue pa-

rameter c. It can be written in the form:

$$\phi(0)\left(U_1''(0) - m\,U_2''(0)\right) = \tilde{c}\left[m\left(\phi_2''(0) + \alpha^2\phi(0)\right) - \left(\phi_1''(0) + \alpha^2\phi(0)\right)\right]. \quad (3.51)$$

It will reside both in the coefficient matrix A and B as follows:

$$\phi(0)\left(U_1''(0) - m\,U_2''(0)\right) \longrightarrow A$$

$$m\left(\phi_2''(0) + \alpha^2\phi(0)\right) - \left(\phi_1''(0) + \alpha^2\phi(0)\right) \longrightarrow B.$$

Interface Condition 4 (3.40), normal stress balance, contains the eigenvalue parameter c. The main problem in this equation is that the eigenvalue parameter c appears nonlinearly. It can be avoided by replacing $1/\tilde{c}$ term in

$$-i\alpha R\left(\frac{1}{Fr} + \frac{\alpha^2}{We}\right)\frac{\phi(0)}{\tilde{c}}$$

by using (3.50):

$$\frac{\phi(0)}{\tilde{c}} = -\frac{\phi_1'(0) - \phi_2'(0)}{U_1'(0) - U_2'(0)}. \quad (3.52)$$

Substituting (3.52) into (3.40) yields

$$i\alpha Re(r-1)U(0)\phi(0) - \left(\phi_1'''(0) - 3\alpha^2\phi_1'(0)\right) + m\left(\phi_2'''(0) - 3\alpha^2\phi_2'(0)\right) - i\alpha Re\left(\frac{\phi_1'(0) - \phi_2'(0)}{U_1'(0) - U_2'(0)}\right)\left[\frac{1}{Fr} + \frac{\alpha^2}{We}\right] = \tilde{c}\, i\alpha Re\left(\phi_1'(0) - r\phi_2'(0)\right). \quad (3.53)$$

It will reside both in the coefficient matrix A and B as follows:

$$i\alpha Re(r-1)U(0)\phi(0) - \left(\phi_1'''(0) - 3\alpha^2\phi_1'(0)\right) + m\left(\phi_2'''(0) - 3\alpha^2\phi_2'(0)\right) - i\alpha Re\left(\frac{\phi_1'(0) - \phi_2'(0)}{U_1'(0) - U_2'(0)}\right)\left[\frac{1}{Fr} + \frac{\alpha^2}{We}\right] \longrightarrow A$$

and

$$i\alpha Re\left(\phi_1'(0) - r\phi_2'(0)\right) \longrightarrow B.$$

3.3.3 Elimination and Conditioning of Matrices

The equation system is well-posed, as it is mentioned before. In order to accommodate those conditions not containing the eigenvalue parameter c in the system, the corresponding rows of the matrix B are zeroed. As a consequence, the matrix B is rendered singular. Therefore, the eigensolver algorithms will result in infinite eigenvalues and corrupt those finite eigenvalues. As a remedy, the corresponding equations are removed from the system and after the computation of the acceptable eigensolutions, those removed equations are accounted for in order to correct the eigenvectors back to the original form [42].

The elimination procedure may create an ill-conditioned matrix system. The error of eigensolution algorithms is generally related to the norm of matrices. Balancing algorithms can be used to decrease the norm of matrices. After balancing operation, matrices and eigenvectors have changed. However, eigenvalues are still the same eigenvalues before conditioning. Therefore, after eigensolution, eigenvector has to be corrected by reversing the steps taken in the balancing operation [65, 66, 67].

Conditioning should be applied when it is necessary. Eigensolvers in this work are third-party codes that are heavily tested and validated against many problems in both literature and industry. For example, MATLAB's "eig" command applies the conditioning option if it decides it is necessary for the problem at hand. Similarly, Octave's "eig" command use conditioning in [67].

3.3.4 Eigensolution and Eigenvectors

MATLAB programming language is chosen to write the code in this work [68]. High-level language benefits, simplicity, built-in mathematical operations, and integrated post-processing tools are some of the reasons in choosing MATLAB. "eig" command of MATLAB is used for the solution of generalized eigenvalue problem. "eig" command is actually templated and overloaded function inside the MATLAB language. Matrices with different properties such as complex, non-complex and generalized, non-generalized eigenvalue problems can be solved via "eig" command.

A similar code is also written in C++ programming language because of lack of independent memory and pointer operations of MATLAB. An external library is decided to be used in order to solve the generalized eigenvalue problem. "Eigen Library" is tried [69]; however, it is observed that solutions of complex generalized eigenvalue problems can not be obtained via "Eigen". Therefore, a different C++ library called "Armadillo" is used for the solution [70]. "Armadillo" is a C++ library for the solution of basic and advanced linear algebraic problems.

Least Stable Eigenvalue

Solution of the generalized eigenvalue problem provides a set of eigenvalues and eigenvectors. Recall that all stable eigenvalues have a negative value. Therefore, the least stable mode in the temporal spectrum Λ, whose value is the one nearest to 0 or already has a positive value:

$$\begin{aligned} \Lambda &= (\lambda_1, \lambda_2, ..., \lambda_{last}) \\ c &= \lambda_{least} = max(imaginary(\Lambda)) \end{aligned} \tag{3.54}$$

Eigenvectors

Grid functions based on the Chebyshev polynomial expansion of streamfunction amplitude $\phi(y)$ is obtained as eigenvectors of the eigenvalue problem. Using (2.36):

$$\phi(y) \approx \sum_{i=0}^{N} \phi_i L_i(y).$$

streamfunction amplitude can be interpolated based on Chebyshev polynomials using the grid values. The value of the least stable temporal eigenvalue, c, is obtained using the eigensolver. Therefore, the corresponding streamfunction can be constructed by using (2.18) and (2.20):

$$\varphi(x, y, t) = \phi(y) e^{i(\alpha x - ct)},$$

$$u'(x, y, t) = \frac{\partial \varphi(x, y, t)}{\partial y},$$

$$v'(x, y, t) = -\frac{\partial \varphi(x, y, t)}{\partial x}.$$

In the case of the multifluid, the grid function representing the amplitudes of the streamfunction corresponding to the least stable eigenvalue contains information on

the two fluids. After the eigenvectors are computed, this information has to be split between the fluids again and the corresponding flow field is computed using

$$u_1 = \frac{\partial \varphi_1}{\partial x} = i\alpha\phi_1\left(y\right)e^{i\alpha(x-ct)},$$

$$u_2 = \frac{\partial \varphi_2}{\partial x} = i\alpha\phi_2\left(y\right)e^{i\alpha(x-ct)},$$

$$v_1 = \frac{\partial \varphi}{\partial y} = \phi_1\left(y\right)' e^{i\alpha(x-ct)},$$

$$v_2 = \frac{\partial \varphi}{\partial y} = \phi_2\left(y\right)' e^{i\alpha(x-ct)}. \tag{3.55}$$

3.3.5 Calculation of Pressure Perturbation Term

The equation for the amplitude of the pressure perturbation term is given by (3.31). During the derivation of the Orr-Sommerfeld equation, this term is eliminated [27]. However, it can be recovered after the solution of the eigenvalue problem.

If the amplitude $\phi(y)$ of the streamfunction is obtained and the temporal eigenvalue c is calculated, the streamfunction $\varphi(x, y, t)$ can be constructed. It is then used to obtain the pressure perturbations using [42]:

$$p_1(x,y,t) = -\left(U_1 - c\right)\varphi_1^{'} + U_1^{'}\varphi_1 + \frac{1}{i\alpha R}\left(\varphi_1^{'''} - \alpha^2\varphi_1^{'}\right) \tag{3.56}$$

$$p_2(x,y,t) = r\left[-\left(U_2 - c\right)\varphi_2^{'} + U_2^{'}\varphi_2 + \frac{m}{i\alpha Rr}\left(\varphi_2^{'''} - \alpha^2\varphi_2^{'}\right)\right] \tag{3.57}$$

CHAPTER 4

VALIDATION TEST CASES AND RESULTS

Preliminary Information

In the following, the assessment of the validity and accuracy of the computations, namely the imaginary part of the eigenvalue parameter c, Im$\{c\}$, are done based on the error measure:

$$\epsilon = \left|\text{Im}\{c_{\text{computed}}\} - \text{Im}\{c_{\text{literature}}\}\right|. \tag{4.1}$$

The computations are tested for grid independency by varying the resolution parameter for single- $K = N$ and two-fluid $K = N + M$ cases until no change in the digits shown in tables are observed. The highest value of K reached through this process is shown in the Tables.

4.1 One Fluid Stability Test Cases

For validation of the computations, tests are performed for single fluid case using three different mean velocity profiles $U(y)$:

- Poiseuille: $U(y) = 1 - y^2$
- Couette: $U(y) = y$
- Boundary Layer (tanh): $U(y) = \tanh(by)$

These profiles are shown in Figure 4.1 below:

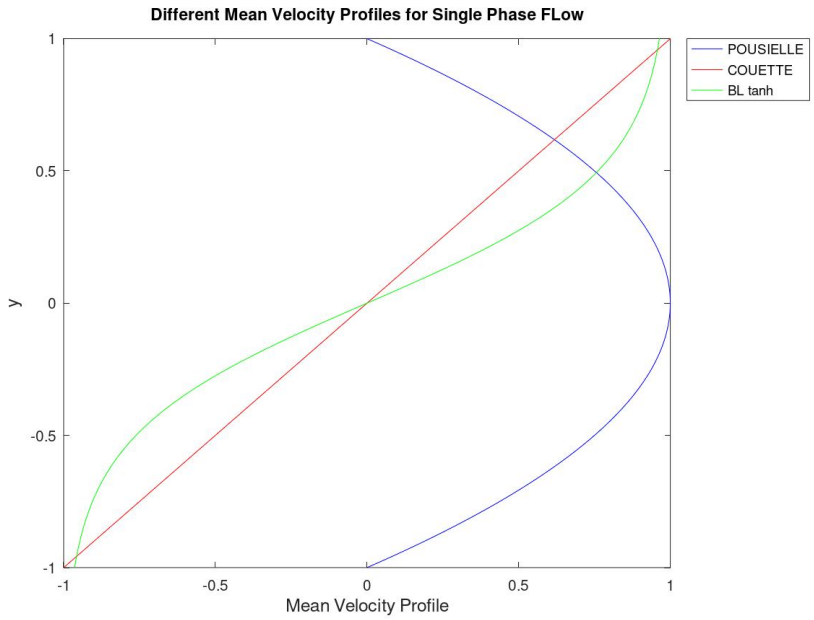

Figure 4.1: Different Mean Velocity Profiles for Single Phase Flows

4.1.1 Poiseuille Flow Test Case

The flow parameters used in ([21], [22], [23]) for the computational stability study of Poiseuille flow in a 2D channel with

$$U(y) = 1 - y^2, \qquad y \in [\,-1\,,\,1\,]$$

are listed in Table 4.1.

Table 4.1: Flow Parameters for Poiseuille Flow Test Case

	Re	α	K
Orszag [21]	5772	1.02	50
Kaffel [22]	10000	1.0	200
Hooper [23]	3000	1.0	80

The computed least stable eigenvalues are compared against the corresponding computational results from the references listed in Table 4.1. The comparison of the computed results are shown in Table 4.2.

Table 4.2: Comparison of Results for Poiseuille Flow Test Case ((n) denotes 10^n)

	$c_{\text{literature}}$	c_{computed}	K	ϵ
Orszag [21]	$0.264 - i\,0.31(-7)$	$0.264 - i\,0.70(-5)$	100	$0.70(-5)$
Kaffel [22]	$0.238 + i\,0.374(-2)$	$0.238 + i\,0.374(-2)$	120	$0.83(-7)$
Hooper [23]	$0.293 - i\,0.10(-1)$	$0.293 - i\,0.10(-1)$	100	$0.10(-6)$

The marginal curve, that is the locus of points with $\text{Im}\{c\} = 0$ in Re versus α frame, separating linearly stable and unstable regions for Poiseuille flow is shown in Figure 4.2 in order to provide a perspective on the values in Tables 4.1 and 4.2.

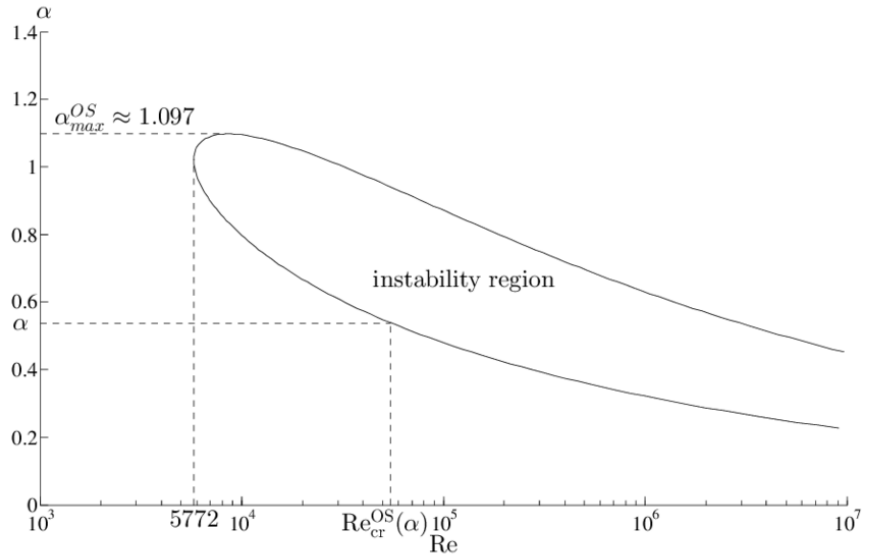

Figure 4.2: The Marginal Curve for Poiseuille Flow [20]

The computed eigenvalue spectrum corresponding to each test case are shown in Figures 4.3, 4.4, and 4.5.

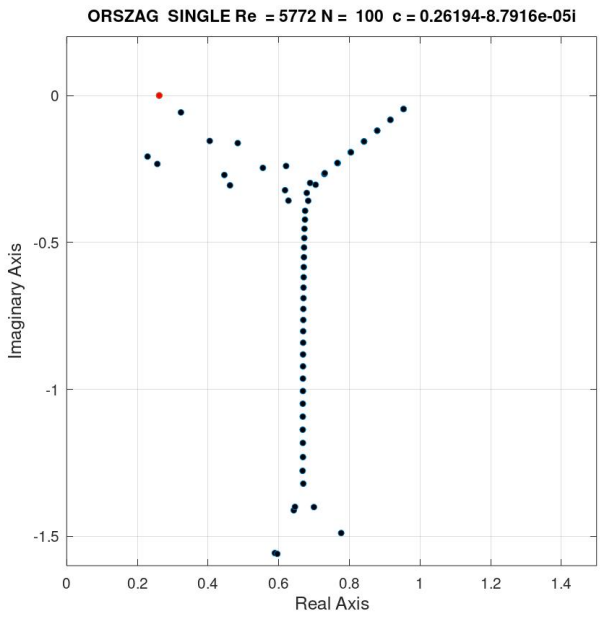

Figure 4.3: Eigenvalues of Poiseuille Flow Test Case: Orszag [21]

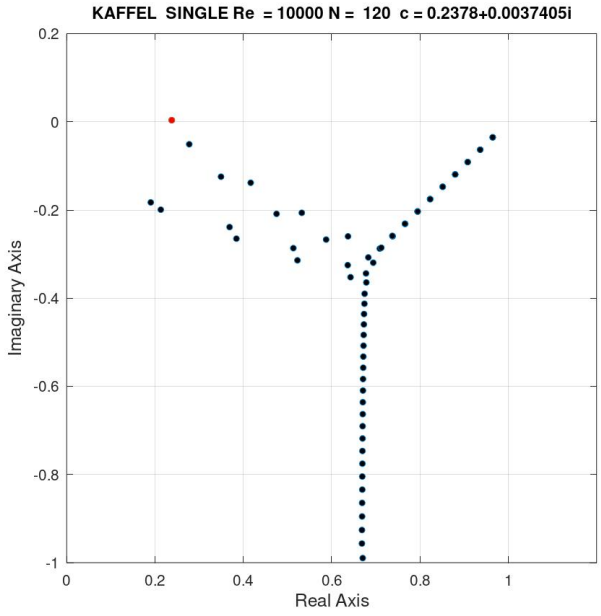

Figure 4.4: Eigenvalues of Poiseuille Flow Test Case: Kaffel [22]

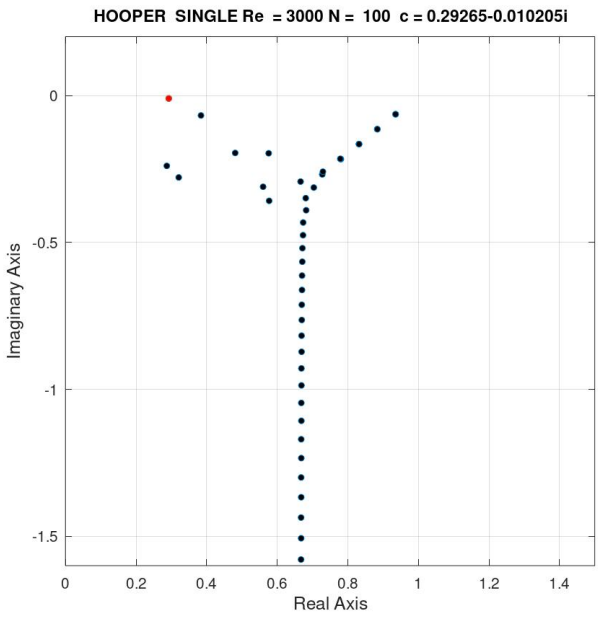

Figure 4.5: The Eigenvalue Spectrum of Poiseuille Flow Test Case: Hooper [23]

4.1.2 Couette Flow Test Case

The flow parameters used ([23]) for the computational stability study of Couette flow between top and bottom lids moving in the opposite directions with

$$U(y) = y, \qquad y \in [\,-1\,,\,1\,]$$

is listed in Table 4.3.

Table 4.3: The Flow Parameters of Couette Flow Test Case

	Re	α	K
Hooper [23]	1500	1.0	80

The computed least stable eigenvalues are compared against the corresponding computational results from the reference listed in Table 4.3. The comparison of the computed results are shown in Table 4.4.

Table 4.4: Comparison of Results for Couette Flow Test Case

	$c_{\text{literature}}$	c_{computed}	K	ϵ
Hooper [23]	$0.653 - i\,0.102$	$0.653 - i\,0.103$	100	$0.13(-4)$

The computed eigenvalue spectrum corresponding to the test case is shown in Figure 4.6.

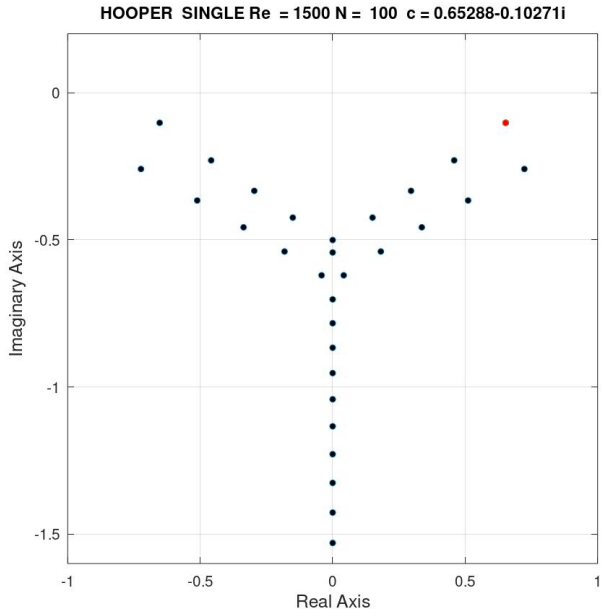

Figure 4.6: The Eigenvalue Spectrum of Couette Flow Test Case [23].

4.1.3 Boundary Layer (tanh) Test Case

This case is similar to Couette flow test case. Only difference is the mean velocity profile. Shear flow is established using symmetric Boundary Layer profile between $y \in [-1, 1]$. The flow parameters used ([2]) for the computational stability study of Boundary Layer flow between top and bottom open boundaries with

$$U(y) = \tanh(by), \qquad y \in [\,-1\,,\,1\,]$$

is listed in Table 4.5. Here, the computational domain is truncated to $[\,-1\,,\,1\,]$.

Table 4.5: The Flow Parameters of Boundary Layer (tanh) Test Case

	Re	α	K
Tang [2]	10, 100, 1000	1.0	100

The computed least stable eigenvalues are compared against the corresponding computational results from the references listed in Table 4.5. The comparison of the computed results are shown in Table 4.2.

Table 4.6: Comparison of Results for Boundary Layer (tanh) Test Case [2]

Re	b	K	$c_{\text{literature}}$	c_{computed}	ϵ
10	2	100	$0.0 - i\,0.851$	$-0.108(-8) - i\,0.852$	$0.51(-3)$
10	8	100	$0.0 - i\,0.684$	$-0.227(-6) - i\,0.685$	$0.57(-3)$
100	2	100	$0.0 + i\,0.154$	$-0.149(-8) + i\,0.154$	$0.67(-4)$
100	8	100	$0.0 + i\,0.449$	$0.572(-9) + i\,0.449$	$0.11(-3)$
1000	2	100	$0.0 + i\,0.164$	$-0.170(-9) + i\,0.164$	$0.11(-3)$
1000	8	100	$0.0 + i\,0.701$	$0.581(-10) + i\,0.701$	$0.16(-4)$

The computed eigenvalue spectrum corresponding to the test case is shown in Figures 4.7 and 4.8.

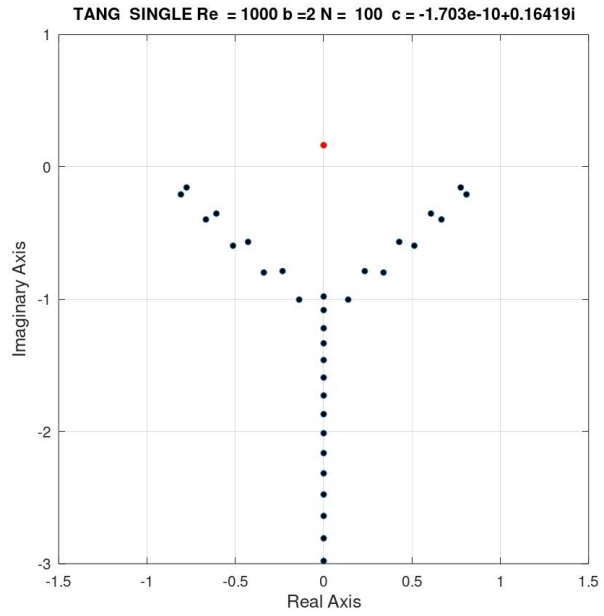

Figure 4.7: The Eigenvalue Spectrum of Boundary Layer Test Case [2] ($Re = 1000$, $\alpha = 1.0$, $K = 100$, $b = 2$).

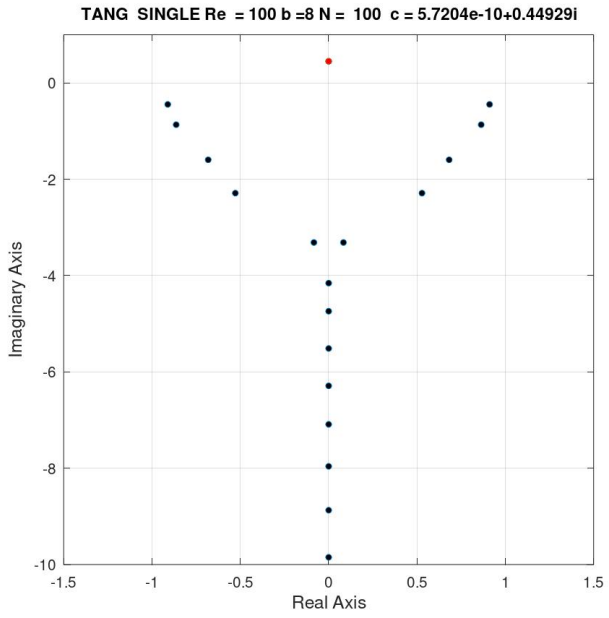

Figure 4.8: The Eigenvalue Spectrum of Boundary Layer Test Case [2] ($Re = 1000$, $\alpha = 1.0$, $K = 100$, $b = 8$).

4.2 Two-fluid Stability Test Cases

Two flow test cases are used to implement the numerical procedure for two-fluid cases. These are:

- Poiseuille
- Couette

4.2.1 Two-fluid Poiseuille Flow Test Case

This test case is the Poiseuille flow of two-fluids in a 2D channel separated by an interface. Different viscosity ratios are implemented in the tests in order to capture the effect of viscosity stratification [22].

The flow parameters for the test cases are shown in Table 4.7. Fluid 1 is confined between the top wall and the interface ($0 \leq y \leq 1$) having the mean velocity profile:

$$U_1(y) = 1 + \frac{m - n^2}{n(1+n)}y - \frac{m+n}{n(1+n)}y^2,$$

while Fluid 2 is between the bottom wall and the interface ($-n \leq y \leq 0$) and have the mean velocity profile:

$$U_2(y) = 1 + \frac{m - n^2}{mn(1+n)}y - \frac{m+n}{mn(1+n)}y^2,$$

where m and n denote viscosity and height ratios, respectively. These parameters and those in Table 4.7 are varied in the tests.

Table 4.7: Flow Parameters (see (3.10))

	Re	α	m	r	n	$1/Fr$	$1/We$
Case 1	10000	1.0	1.0	1.0	1.0	0.0	0.0
Case 2	10000	1.0	0.5	1.0	1.0	0.0	0.0

The combined mean velocity profile is shown in Figure 4.9 for some viscosity ratio (m) values.

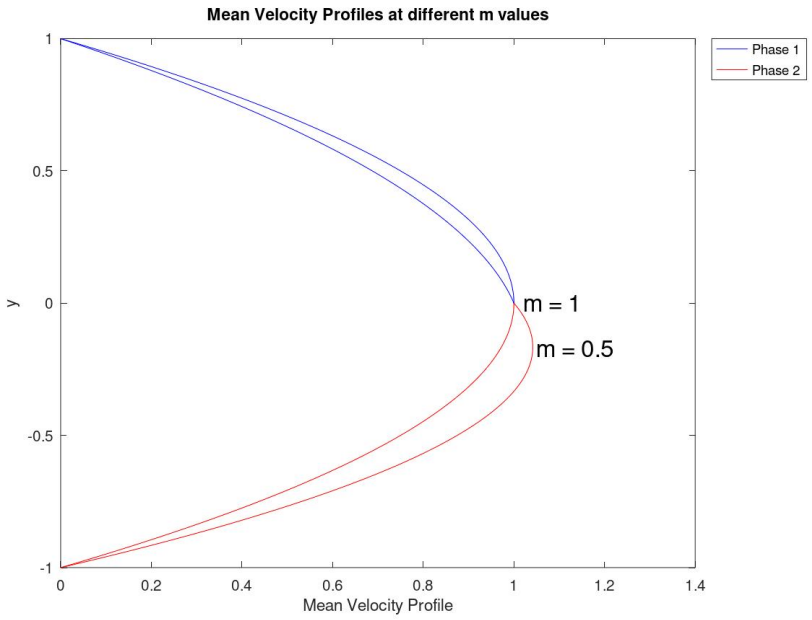

Figure 4.9: Combined Mean Velocity Profiles of Two-fluid Poiseuille Flow with m

The computed least stable eigenvalues are compared against the corresponding computational results in [22]. The comparison of the computed results are shown in Table 4.8.

Table 4.8: Comparison of Results for Multiphase Poiseuille Test Cases

	$N+M$	$c_{\text{literature}}$	c_{computed}	ϵ
Case 1	$100+100$	$0.238+i\,0.374(-2)$	$0.238-i\,0.374(-2)$	$0.70(-6)$
Case 2	$100+100$	$0.999-i\,0.10(-8)$	$1.0+i\,2.55(-6)$	$2.55(-6)$

4.2.1.1 The Case $m = 1$

This is actually a test case for the virtual interface algorithm. A virtual interface is a transparent interface placed within a single fluid. In this case

$$U_1^{'}(0) = U_2^{'}(0) \qquad \text{and} \qquad U_1^{''}(0) = U_2^{''}(0).$$

These will reduce 2nd and 3rd Interface Conditions (3.38, 3.39) to

$$\phi_1^{'}(0) = \phi_2^{'}(0) \qquad \text{and} \qquad \phi_1^{''}(0) = \phi_2^{''}(0) \tag{4.2}$$

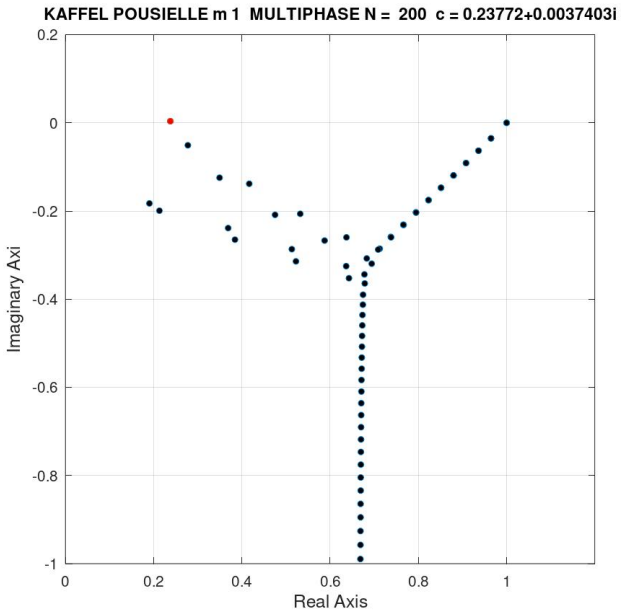

Figure 4.10: The Eigenvalue Spectrum of Poiseuille Flow Test Case 1.

If, in addition, ($r = 1$), inverse Froude and Weber numbers are 0, then 4th Interface Condition also reduces to

$$\phi_1'''(0) = \phi_2'''(0) \tag{4.3}$$

Thus, in addition to the boundary conditions, the (virtual) interface conditions do not contain the eigenvalue parameter c. As a result, the corresponding rows in the B matrix are eliminated in order to remove the singularity of the matrix. The corresponding eigenvalue spectrum is shown in Figure 4.10, where the typical **Y** shape, a signature spectrum of one fluid Poiseuille flow, appears.

4.2.1.2 The Case $m = 0.5$

In this case, only simplification due to $r = 1$ occurs in the 4th Interface Condition where the eigenvalue parameter c is removed. The corresponding eigenvalue spectrum is shown in Figure 4.11, where the typical **Y** shape now appears in tandem.

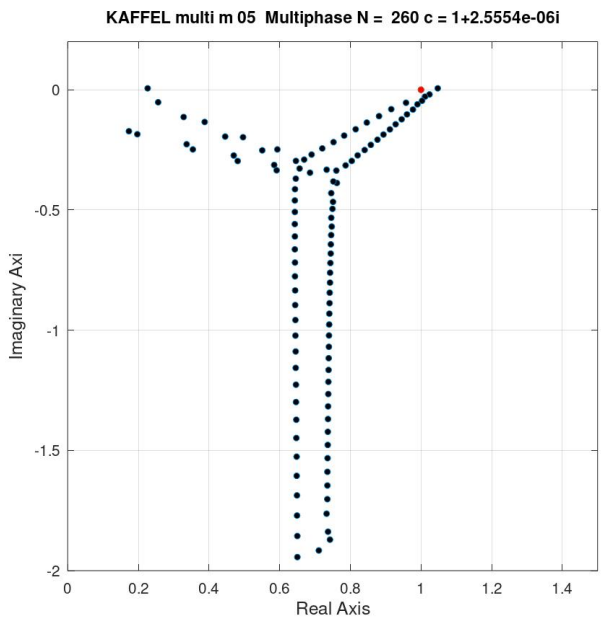

Figure 4.11: The Eigenvalue Spectrum of Poiseuille Flow Test Case 2.

4.2.2 Two-Fluid Couette Flow Test Case

In this case, Couette flow is split into two parts by an interface separating two fluids. Different viscosity ratios are implemented in the tests in order to capture the effect of viscosity stratification [30].

The flow parameters for the test cases are shown in Table 4.9. Fluid 1 is confined between the top moving lid and the interface ($0 \leq y \leq 1$) having the mean velocity profile:

$$U_1(y) = \frac{my + n}{m + n},$$

while Fluid 2 is between the bottom moving lid and the interface ($-n \leq y \leq 0$) and have the mean velocity profile:

$$U_2(y) = \frac{y + n}{m + n}.$$

These parameters and those in Table 4.7 are varied in the tests.

Table 4.9: Interface Properties

	Re	α	m	r	n	$1/Fr$	$1/We$
Case 1	1200	1.0	0.2	1.0	1.0	0.0	0.0
Case 2	2500	1.0	1.5	1.0	1.0	0.0	0.0
Case 3	6000	1.0	2.0	1.0	1.0	0.0	0.0

The combined mean velocity profile is shown in Figure 4.12 for some viscosity ratio (m) values.

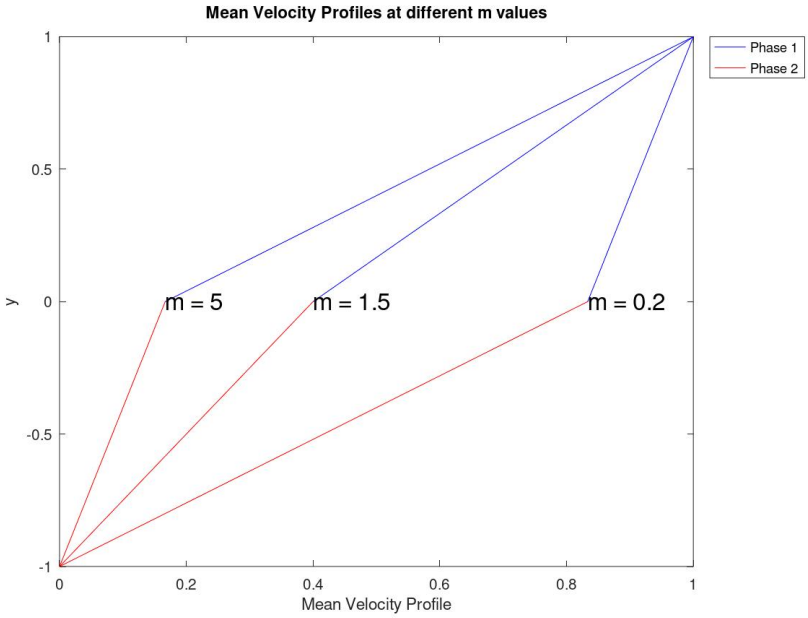

Figure 4.12: Combined Mean Velocity Profiles of Two-fluid Couette Flow with m

The computed least stable eigenvalues are compared with the reference least stable eigenvalues [30]. The comparison results are presented in Table 4.10.

Table 4.10: Comparison of Results for Multiphase Couette Test Cases

	$N+M$	$c_{\text{literature}}$	c_{computed}	ϵ
Case 1	$80+80$	$0.85+i\,0.00$	$0.833+i\,0.325(-7)$	$0.32(-7)$
Case 2	$80+80$	$0.41+i\,0.0$	$0.40-i\,0.696(-9)$	$0.70(-9)$
Case 3	$80+80$	$0.16+i\,0.0$	$0.167+i\,0.766(-7)$	$0.77(-7)$

The corresponding eigenvalue spectrum is shown in Figures 4.13, 4.14, and 4.15.

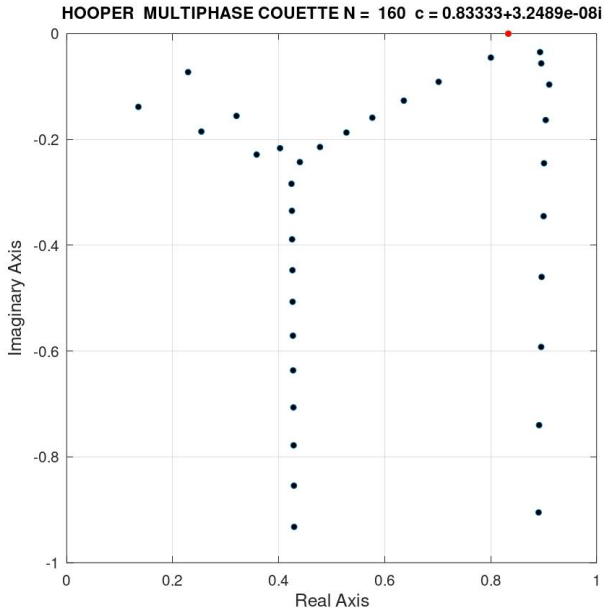

Figure 4.13: The Eigenvalue Spectrum of Couette Flow Test Case 1.

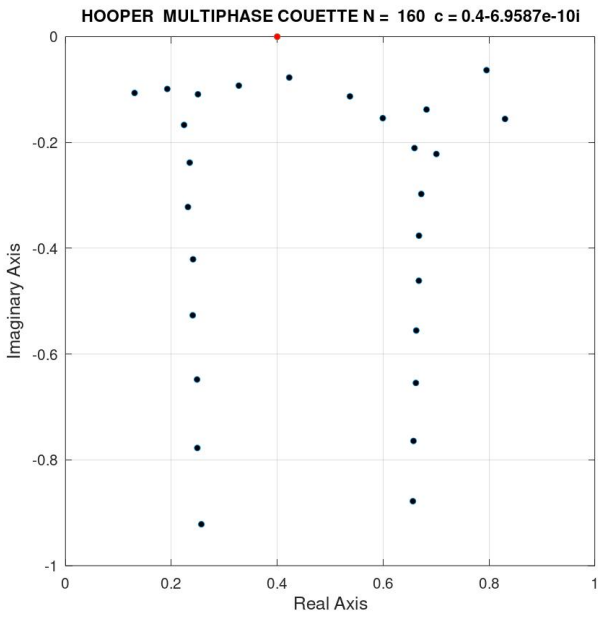

Figure 4.14: The Eigenvalue Spectrum of Couette Flow Test Case 2.

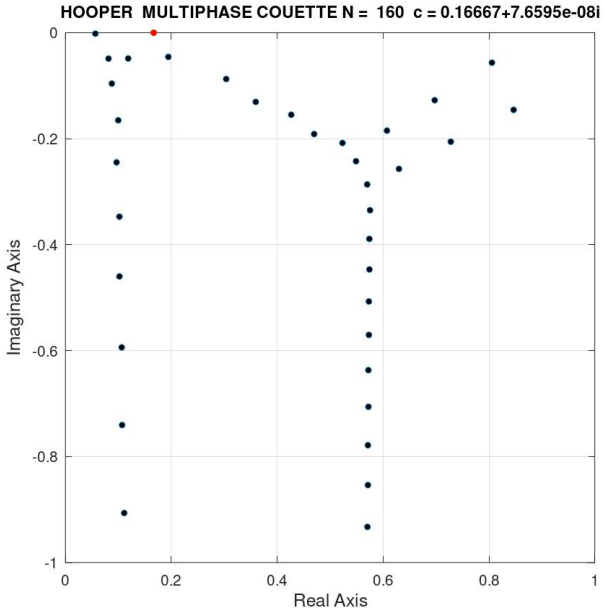

Figure 4.15: The Eigenvalue Spectrum of Couette Flow Test Case 3.

CHAPTER 5

DISCUSSION AND CONCLUSIONS

Instabilities which are originated from interfaces are still an active research area. In this study, the single-fluid and two-fluid stability of flow configurations are investigated. The Navier-Stokes equations modelling the flow of viscous fluids are linearized and transformed into Orr-Sommerfeld stability equation via linear hydrodynamic stability theory[1]. Temporal stability is studied in both single-fluid and two-fluid flows. In order to solve the Orr-Sommerfeld equation with high accuracy, Spectral method (Chebyshev Collocation Method) is used.

For linear stability study of single-fluid flow configurations, Couette, Boundary Layer (tanh) and Poiseuille mean velocity profiles are used to validate the mathematical formulation and computational implementation [21, 22, 23, 2]. The computer code developed is validated for all configurations as presented in Chapter 4. After passing these single-fluid test cases, two-fluid Orr-Sommerfeld equations, boundary and interface conditions are derived. Domain decomposition method is chosen for the two-fluid flow configuration [33]. Pre-processing in the form of row and column elimination of the system matrices are performed on the resulting algebraic generalized eigenproblem. Conditioning is used during the computation of the eigensolutions. The effects of the mean velocity profiles and dimensionless physical parameters are observed in two-fluid test cases. Poiseuille and Couette mean velocity profiles are used in two-fluid configurations with different viscosity ratios. The computed results are validated using the studies in [30], [22] satisfactorily in Chapter 4.

The eigenvalue spectrum associated with the linear stability analysis of the Poiseuille flow has the typical **Y** shape extending below the real axis whose lower part is associated with the dissipative processes and upper part are associated with the convective

processes.

When the two fluid separated by the interface have the same physical parameters, such as viscosity, density, then the interface is a virtual one and it fact the flow configuration corresponds to one-fluid case. The computer code developed for the two-fluid Poiseuille flow case is tested in this case of virtual interface and compared with the one-fluid Poiseuille case successfully resulting in the typical **Y** shaped eigenvalue spectrum as shown in Figure 4.10. When the viscosity ratio is changed to $m = 0.5$, the **Y** shaped eigenvalue spectrum is split into two as shown in Figure 4.11. This is reflecting the fact that each **Y** shaped spectrum corresponds to one of the fluids separated by the interface. This provides additional control parameters to study the effects of various physical parameters on the linear stability of the underlying flow configuration. This opens the way to understand the stability phenomena in more depth that was not possible in the time constraint of this study. It remains as a future study.

The effects of introducing an interface separating two different fluids on the linear stability eigenvalue spectrum are observed as shift between convective and diffusive effects in the case of Couette flow configuration in Figures 4.13, 4.14, and 4.15. They show that when the viscosity ratio is at low level ($m = 1.5$), convective and diffusive eigenvalues can be observed for each fluid. However, for the high level viscosity ratios ($m = 0.2$, $m = 5$) only dissipative eigenvalues are apparent for the fluid with high viscosity. Most unstable eigenvalue is shifted towards the high viscosity fluid.

This study can be considered as a preliminary and exploratory study on the two-fluid flow instabilities as much as can be done in the time constraints of a Master Thesis. As possible future work, the following items may be considered:

- Effect of Compressibility:

  Incompressibility assumption, which is assumed at the beginning of the derivation of Orr-Sommerfeld Equations, can be removed. The compressible version of the governing equations can be derived, and acoustic effects can be included in the interface condition. Compressible - Compressible cases may be investigated. Thus, instabilities that occur in astrophysics or inertial confinement fusion can be studied. Compressible - Incompressible cases are more com-

mon in real-life applications such as air over ocean, gas shearing liquid film. Gas can be considered as incompressible at low velocities, as it is done in this study. However, suppose the velocity of the gas is high enough to consider the comppressibility effects such as acoustic phenomena.

- Investigation of Spatial Instability

  In this study temporal instability is investigated. Spatial instability of the two-phase flow problems can be investigated. However, the resulting eigenproblem comes out to be nonlinear. Therefore, study of spatial instability will be more difficult in comparison to study of temporal instability.

- Classification of Instabilities

  As it is mentioned before, the instability of two-fluid flows is not only dependent on the Reynolds number. In order to classify the instabilities, the effects of the dominant physics in the two-phase flow system have to be compared. Energy methods [71] can be used to calculate the global change (increase or decrease) in perturbation energies. Energy levels associated with the Reynolds stresses and viscous stresses will be similar to single-fluid case and generally depends on the Reynolds number. The instabilities in the two-fluid case are generally generated by the interfacial effects. Dominant increase in the energy levels will define the instability type. For example, if the effect of gravity due to density stratification is dominant, instability can be classified as Rayleigh-Taylor Instability [33].

  The problem with the classification using energy methods is that sometimes there is no unique dominant physical effect. This will create coupling of physical effects, and determining the source will be more difficult.

- Nonlinear Hydrodynamic Stability

  As it is mentioned in Chapter 2, if the amplitude of the perturbations is increased and decoupling is no longer valid, then the system becomes nonlinear and the nonlinear effects become dominant. Therefore, the linear theory will not be enough to capture the evolution of instabilities. As a relatively easier transition to the nonlinear problem, a weakly nonlinear problem may be considered.

- GUI Development

  A GUI (graphical user interface) can be developed. GUI will help both developers and users to study the effects of new physical effects such as heat transfer, phase change, magnetic field, etc. Some of the physical problems may include more than two fluid layers [42]. Construction of multi-fluid stability matrix and implementation of interface conditions with additional dimensionless physical parameters may be incorporated in GUI.

REFERENCES

[1] P. G. Drazin and W. H. Reid, *Hydrodynamic stability*. Cambridge university press, 2004.

[2] J. Tang, *STABILITY STUDY ON SHEAR FLOW AND VORTICES IN LATE BOUNDARY LAYER TRANSITION*. PhD thesis, 2017.

[3] M. S. Roberts, *Experiments and simulations on the incompressible, Rayleigh-Taylor instability with small wavelength initial perturbations*. PhD thesis, The University of Arizona, 2012.

[4] M. S. Roberts, "Fluid instabilities and transition to turbulence," in *Fluid-Structure Interaction*, IntechOpen, 2020.

[5] R. L. Holmes, G. Dimonte, B. Fryxell, M. L. Gittings, J. W. Grove, M. Schneider, D. H. Sharp, A. L. Velikovich, R. P. Weaver, and Q. Zhang, "Richtmyer–meshkov instability growth: experiment, simulation and theory," *Journal of Fluid Mechanics*, vol. 389, pp. 55–79, 1999.

[6] P. C. Philippi, K. K. Mattila, L. A. Hegele Júnior, and D. N. Siebert, "Kinetic projection and stability in lattice-boltzmann schemes," 2015.

[7] L. Boegman, "Currents in stratified water bodies 2: Internal waves," *Encyclopedia of inland waters*, vol. 1, pp. 539–558, 2009.

[8] I. Zhelyazkov and R. Chandra, *Kelvin–Helmholtz Instability in Solar Atmospheric Jets*. World Scientific, 2021.

[9] C. Inoue and I. Maeda, "On the droplet entrainment from gas-sheared liquid film," *Physics of Fluids*, vol. 33, no. 1, p. 011705, 2021.

[10] S. S. Jain, A. Mani, and P. Moin, "A conservative diffuse-interface method for compressible two-phase flows," *Journal of Computational Physics*, vol. 418, p. 109606, 2020.

[11] K. Taira, S. L. Brunton, S. T. Dawson, C. W. Rowley, T. Colonius, B. J. McKeon, O. T. Schmidt, S. Gordeyev, V. Theofilis, and L. S. Ukeiley, "Modal analysis of fluid flows: An overview," *Aiaa Journal*, vol. 55, no. 12, pp. 4013–4041, 2017.

[12] J. Herman and M. Baram, "In the midst of turbulence, heliox kept her alive," *Annals of the American Thoracic Society*, vol. 14, no. 3, pp. 452–455, 2017.

[13] H. Schlichting and K. Gersten, *Boundary-layer theory*. Springer Science & Business Media, 2003.

[14] J. P. Boyd, *Chebyshev and Fourier spectral methods*. Courier Corporation, 2001.

[15] S. Kandlikar, S. Garimella, D. Li, S. Colin, and M. R. King, *Heat transfer and fluid flow in minichannels and microchannels*. elsevier, 2005.

[16] K. Heijmans, A. D. Pathak, P. Solano-López, D. Giordano, S. Nedea, and D. Smeulders, "Thermal boundary characteristics of homo-/heterogeneous interfaces," *Nanomaterials*, vol. 9, no. 5, p. 663, 2019.

[17] P. M. Schweizer and S. Kistler, *Liquid Film Coating: Scientific principles and their technological implications*. Springer Science & Business Media, 2012.

[18] I. Barmak, A. Gelfgat, H. Vitoshkin, A. Ullmann, and N. Brauner, "Stability of stratified two-phase flows in horizontal channels," *Physics of Fluids*, vol. 28, no. 4, p. 044101, 2016.

[19] H. E. Krogstad and O. A. Arntsen, "Linear wave theory part a," *Norwegian University of Science and Technology*, pp. 5–9, 2000.

[20] K. V. Demyanko and Y. M. Nechepurenko, "Linear stability analysis of poiseuille flow in a rectangular duct," *Russ. J. Numer. Anal. Math. Modelling*, vol. 28, no. 2, pp. 125–148, 2013.

[21] S. A. Orszag, "Accurate solution of the orr–sommerfeld stability equation," *Journal of Fluid Mechanics*, vol. 50, no. 4, pp. 689–703, 1971.

[22] A. Kaffel and A. Riaz, "Eigenspectra and mode coalescence of temporal instability in two-phase channel flow," *Physics of Fluids*, vol. 27, no. 4, p. 042101, 2015.

[23] A. Hooper and R. Grimshaw, "Two-dimensional disturbance growth of linearly stable viscous shear flows," *Physics of Fluids*, vol. 8, no. 6, pp. 1424–1432, 1996.

[24] D. A. Drew and S. L. Passman, *Theory of multicomponent fluids*, vol. 135. Springer Science & Business Media, 2006.

[25] T. B. Benjamin, "Wave formation in laminar flow down an inclined plane," *Journal of Fluid Mechanics*, vol. 2, no. 6, pp. 554–573, 1957.

[26] C.-S. Yih and C. Guha, "Hydraulic jump in a fluid system of two layers," *Tellus*, vol. 7, no. 3, pp. 358–366, 1955.

[27] C.-S. Yih, "Instability due to viscosity stratification," *Journal of Fluid Mechanics*, vol. 27, no. 2, pp. 337–352, 1967.

[28] C.-S. Yih, "Wave formation on a liquid layer for de-icing airplane wings," *Journal of Fluid Mechanics*, vol. 212, pp. 41–53, 1990.

[29] C.-S. Yih, "Stability of two-dimensional parallel flows for three-dimensional disturbances," in *Selected Papers By Chia-Shun Yih: (In 2 Volumes)*, pp. 282–283, World Scientific, 1991.

[30] A. Hooper and M. South, "Eigenvalues and disturbance growth in channel flow of two superposed viscous fluids," *Advances in Multi-Fluid Flows. SIAM*, pp. 271–287, 1996.

[31] A. Hooper and W. Boyd, "Shear-flow instability at the interface between two viscous fluids," *Journal of Fluid Mechanics*, vol. 128, pp. 507–528, 1983.

[32] A. Hooper and W. Boyd, "Shear-flow instability due to a wall and a viscosity discontinuity at the interface," *Journal of Fluid Mechanics*, vol. 179, pp. 201–225, 1987.

[33] P. Boomkamp and R. Miesen, "Classification of instabilities in parallel two-phase flow," *International Journal of Multiphase Flow*, vol. 22, pp. 67–88, 1996.

[34] R. Kelly, D. Goussis, S. Lin, and F. Hsu, "The mechanism for surface wave instability in film flow down an inclined plane," *Physics of Fluids A: Fluid Dynamics*, vol. 1, no. 5, pp. 819–828, 1989.

[35] R. Miesen, G. Beijnon, P. Duijvestijn, R. Oliemans, and T. Verheggen, "Interfacial waves in core-annular flow," *Journal of Fluid Mechanics*, vol. 238, pp. 97–117, 1992.

[36] R. Miesen and B. J. Boersma, "Hydrodynamic stability of a sheared liquid film," *Journal of fluid mechanics*, vol. 301, pp. 175–202, 1995.

[37] S. G. Yiantsios and B. G. Higgins, "Linear stability of plane poiseuille flow of two superposed fluids," *The Physics of fluids*, vol. 31, no. 11, pp. 3225–3238, 1988.

[38] B. Ng and W. Reid, "A numerical method for linear two-point boundary-value problems using compound matrices," *Journal of Computational Physics*, vol. 33, no. 1, pp. 70–85, 1979.

[39] B. Ng and W. Reid, "The compound matrix method for ordinary differential systems," *Journal of Computational Physics*, vol. 58, no. 2, pp. 209–228, 1985.

[40] S. Timoshin, "Instabilities in a high-reynolds-number boundary layer on a film-coated surface," *Journal of Fluid Mechanics*, vol. 353, pp. 163–195, 1997.

[41] S. Özgen, G. Degrez, and G. Sarma, "Two-fluid boundary layer stability," *Physics of fluids*, vol. 10, no. 11, pp. 2746–2757, 1998.

[42] P. Boomkamp, B. Boersma, R. Miesen, and G. Beijnon, "A chebyshev collocation method for solving two-phase flow stability problems," *Journal of Computational Physics*, vol. 132, pp. 191–200, 1997.

[43] D. Lecoanet, M. McCourt, E. Quataert, K. J. Burns, G. M. Vasil, J. S. Oishi, B. P. Brown, J. M. Stone, and R. M. O'Leary, "A validated non-linear kelvin–helmholtz benchmark for numerical hydrodynamics," *Monthly Notices of the Royal Astronomical Society*, vol. 455, no. 4, pp. 4274–4288, 2016.

[44] S. Mirjalili, S. S. Jain, and M. Dodd, "Interface-capturing methods for two-phase flows: An overview and recent developments," *Center for Turbulence Research Annual Research Briefs*, vol. 2017, no. 117-135, p. 13, 2017.

[45] M. Wörner, *A compact introduction to the numerical modeling of multiphase flows*, vol. 6932. FZKA, 2003.

[46] R. Saurel and C. Pantano, "Diffuse-interface capturing methods for compressible two-phase flows," *Annual Review of Fluid Mechanics*, vol. 50, pp. 105–130, 2018.

[47] W. O. Criminale, T. L. Jackson, and R. D. Joslin, *Theory and computation in hydrodynamic stability*. Cambridge University Press, 2018.

[48] P. G. Drazin, *Introduction to hydrodynamic stability*, vol. 32. Cambridge university press, 2002.

[49] H. Squires, "On the stability for three-dimensional disturbances of viscous flow between parallel walls," *Proc. R. Soc. Lond. A*, vol. 142, pp. 621–628, 1933.

[50] D. Hsieh and S. Ho, "Wave and stability in fluids," *Journal of Fluid Mechanics*, vol. 312, no. 1, pp. 408–408, 1996.

[51] J. C. Mason and D. C. Handscomb, *Chebyshev polynomials*. CRC press, 2002.

[52] J. Hesthaven, S. Gottlieb, and D. Gottlieb, *Spectral Methods for Time-Dependent Problems*. Cambridge University Press, 2007.

[53] L. N. Trefethen, *Spectral methods in MATLAB*. SIAM, 2000.

[54] S. Bechtel and R. Lowe, *Fundamentals of Continuum Mechanics: With Applications to Mechanical, Thermomechanical, and Smart Materials*. Academic Press, 2014.

[55] E. B. Tadmor, R. E. Miller, and R. S. Elliott, *Continuum mechanics and thermodynamics: from fundamental concepts to governing equations*. Cambridge University Press, 2012.

[56] R. Aris, *Vectors, tensors and the basic equations of fluid mechanics*. Courier Corporation, 2012.

[57] A. J. Chorin, J. E. Marsden, and J. E. Marsden, *A mathematical introduction to fluid mechanics*, vol. 168. Springer, 1990.

[58] J. C. Slattery, L. Sagis, and E.-S. Oh, *Interfacial transport phenomena*. Springer Science & Business Media, 2007.

[59] W. Albring, "Handbuch der physik, band viii/2. strömungsmechanik ii. herausgeber s. flügge, mitherausgeber c. truesdell. vi+ 696 s. m. 177 fig. berlin/göttingen/heidelberg 1963. springer-verlag. preis geb. dm 198,-.," 1964.

[60] I. Barmak, A. Y. Gelfgat, A. Ullmann, and N. Brauner, "On the squire's transformation for stratified two-phase flows in inclined channels," *International Journal of Multiphase Flow*, vol. 88, pp. 142–151, 2017.

[61] U. Schaflinger, "A short note on squire's theorem for interfacial instabilities in a stratified flow of two superposed fluids," *Fluid Dynamics Research*, vol. 14, no. 5, p. 223, 1994.

[62] T. I. Hesla, F. R. Pranckh, and L. Preziosi, "Squire's theorem for two stratified fluids," *The Physics of fluids*, vol. 29, no. 9, pp. 2808–2811, 1986.

[63] S. Whitaker, *Introduction to fluid mechanics*. Prentice-Hall, 1968.

[64] J. C. Slattery, *Advanced transport phenomena*. Cambridge University Press, 1999.

[65] E. Osborne, "On pre-conditioning of matrices," *Journal of the ACM (JACM)*, vol. 7, no. 4, pp. 338–345, 1960.

[66] R. James, J. Langou, and B. R. Lowery, "On matrix balancing and eigenvector computation," *arXiv preprint arXiv:1401.5766*, 2014.

[67] R. C. Ward, "Balancing the generalized eigenvalue problem," *SIAM Journal on Scientific and Statistical Computing*, vol. 2, no. 2, pp. 141–152, 1981.

[68] S. Matlab, "Matlab," *The MathWorks, Natick, MA*, 2012.

[69] G. Guennebaud, B. Jacob, *et al.*, "Eigen," *URl: http://eigen. tuxfamily. org*, vol. 3, 2010.

[70] C. Sanderson and R. Curtin, "Armadillo: a template-based c++ library for linear algebra," *Journal of Open Source Software*, vol. 1, no. 2, p. 26, 2016.

[71] D. D. Joseph and Y. Y. Renardy, *Fundamentals of two-fluid dynamics: Part i: Mathematical theory and applications*, vol. 3. Springer Science & Business Media, 2013.